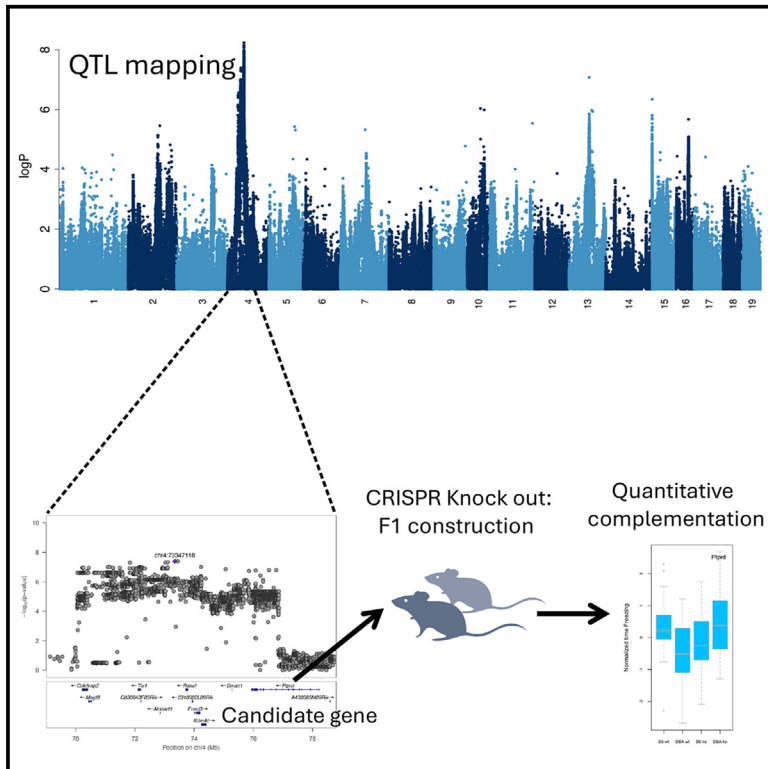# Cell Genomics

Complementation testing identifies genes mediating effects at quantitative trait loci underlying fear-related behavior

Graphical abstract

Authors

Patrick B. Chen, Rachel Chen, Nathan LaPierre, ..., Jason Ernst, Chongyuan Luo, Jonathan Flint

Correspondence

jflint@mednet.ucla.edu

In brief

Chen et al. use quantitative complementation to identify genes at six quantitative trait loci influencing fear-related behaviors. Epigenetic analysis indicated that genetic variation is more permissible in excitatory than inhibitory neuronal circuits. Creating CRISPR knockouts in inbred strains makes it possible to identify genes at QTLs in mice.

Highlights

- Meta-analysis with 6,544 mice found 93 quantitative trait loci for fear-related behavior

- Quantitative complementation testing identified six genes at six quantitative trait loci

- Epigenetic analyses implicated excitatory neurons as mediating the genetic effects

- Genetic variation occurs preferentially in excitatory versus inhibitory neuronal circuits

CellPress

Cell Genomics

Article

Complementation testing identifies genes mediating effects at quantitative trait loci underlying fear-related behavior

Patrick B. Chen,[1] Rachel Chen,[1] Nathan LaPierre,[2,3] Zeyuan Chen,[2] Joel Mefford,[3] Emilie Marcus,[4] Matthew G. Heffel,[3] Daniela C. Soto,[1] Jason Ernst,[2,4] Chongyuan Luo,[3] and Jonathan Flint[1,5,*]

[1]Department of Psychiatry and Biobehavioral Sciences, David Geffen School of Medicine, University of California, Los Angeles, Los Angeles, CA, USA
[2]Department of Computer Science, Samueli School of Engineering, University of California, Los Angeles, Los Angeles, CA, USA
[3]Department of Human Genetics, David Geffen School of Medicine, University of California, Los Angeles, Los Angeles, CA, USA
[4]Department of Biological Chemistry, University of California, Los Angeles, Los Angeles, CA, USA
[5]Lead contact
*Correspondence: jflint@mednet.ucla.edu
https://doi.org/10.1016/j.xgen.2024.100545

SUMMARY

Knowing the genes involved in quantitative traits provides an entry point to understanding the biological bases of behavior, but there are very few examples where the pathway from genetic locus to behavioral change is known. To explore the role of specific genes in fear behavior, we mapped three fear-related traits, tested fourteen genes at six quantitative trait loci (QTLs) by quantitative complementation, and identified six genes. Four genes, *Lamp*, *Ptprd*, *Nptx2*, and *Sh3gl*, have known roles in synapse function; the fifth, *Psip1*, was not previously implicated in behavior; and the sixth is a long non-coding RNA, *4933413L06Rik*, of unknown function. Variation in transcriptome and epigenetic modalities occurred preferentially in excitatory neurons, suggesting that genetic variation is more permissible in excitatory than inhibitory neuronal circuits. Our results relieve a bottleneck in using genetic mapping of QTLs to uncover biology underlying behavior and prompt a reconsideration of expected relationships between genetic and functional variation.

INTRODUCTION

A major challenge in behavior genetics is to turn genetic information into mechanistic understanding of the sort that would, for example, be useful in designing new treatments for psychiatric disorders and, more generally, understanding how genetic variation leads to behavioral variation. A key step is progressing from quantitative trait locus (QTL) to gene, which has only been achieved for any complex trait, in any species, in a small number of cases.[1,2] Of the 5,000 QTLs identified in rodents, less than 100 genes have been identified, almost all on the basis of correlative evidence, such as proximity of a gene to the QTL or alterations in transcript abundance, rather than by a causal test of a gene's candidacy.[2] Currently, there is no consensus on how to proceed from QTL to gene.

Here, we demonstrate the power of a quantitative complementation (QC) test, first applied in *Drosophila*[3] and later shown to work in rodents,[4] to directly query the causal gene impacted by the QTL. Construction and phenotyping of F1 hybrids with and without a knockout (KO) of a candidate gene, and of inbred strains with and without the KO of a candidate gene, test whether the QTL operates through the gene under investigation. By separately assaying the joint effect of QTLs (from the phenotypic difference between strains) and the effect of the mutation (from the phenotypic difference between KOs and wild type [WT]), the QC test reveals a QTL whose effect depends on the presence of the candidate gene as a significant interaction between the effect of mutation and the effect of strain. Applying the test requires access to inbred animals carrying a KO on the same genetic background as the QTL, which has been difficult to achieve when KOs were generated using homologous recombination in 129 strains or C57BL/6N. The development of the CRISPR-Cas9 technology now lifts that restriction by enabling genetic manipulation in any strain.[5,6]

We set out to apply the QC test to fear-related behaviors. We chose these traits because we could use extensive information available about the brain regions involved (ventral hippocampus and amygdala[7,8]), and their underlying circuitry,[9–12] to explore where and how in the brain genetic variation results in behavioral change. We reasoned that by knowing the causal genes, we could identify changes in their expression and regulation at a single-cell level, revealing the molecular mechanisms that mediate the impact of genetic variants on traits.
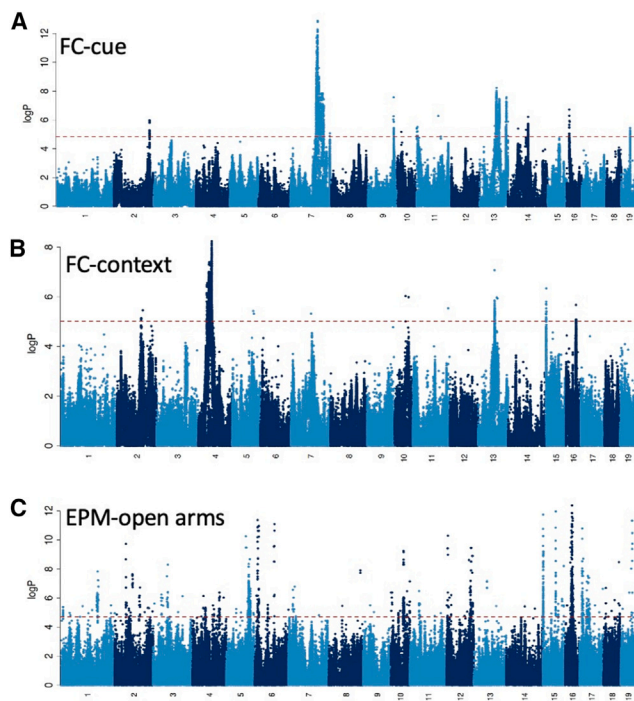
Figure 1. Manhattan plots for three fear-related behaviors in mice
(A–C) The data show the results of a meta-analysis of (A) 1,931 mice for cue conditioning (FC-cue), (B) 2,671 for contextual conditioning (FC-context), and (C) 1,942 for entries into the open arms of the elevated plus maze (EPM-open arms). Chromosome numbers are listed on the horizontal axis. The vertical scale is the negative logarithm (base 10) of the association p value. A horizontal dotted red line gives the location of the 5% significance threshold (from simulation).

RESULTS

Generating a large-scale set of phenotypes and genotypes

Our first task was to identify QTLs involved in fear-related behaviors that ideally indicated one or a small number of genes for QC testing. We chose a hybrid mouse diversity panel (HMDP) for mapping because of its potential to deliver high resolution[2] (thus increasing the chance of finding QTLs containing a small number of candidate genes) and because it includes recombinant inbreds derived from C57BL/6J, hence providing many QTL alleles on a strain readily amenable to CRISPR-Cas9 modification (the HMDP strains and numbers of animals used are listed in Table S1). We mapped variation in a conditioned fear assay in which animals were exposed to an auditory cue associated with an aversive shock. Re-exposure to the auditory cue elicits a fear response, measured as the amount of time spent freezing[13,14] and referred to in this paper as FC-cue. The context in which conditioning occurs also elicits freezing (FC-context),[15] and we assayed this too. We also mapped variation in an unconditioned fear assay using the elevated plus maze (EPM), whose open arms act as anxiogenic environment. We counted the number of entries into the EPM's open arms as a measure of fear, referred to henceforth as EPM-open.

To enable us to perform a well-powered meta-analysis and robustly identify loci at high resolution, we combined our data with results from 29 publications.[16–45] We implemented a rigorous pipeline to harmonize phenotypes across the multiple datasets (STAR Methods: harmonizing phenotyping data for meta-analysis), generating phenotypes on a total of 6,544 mice from seven cohorts (Tables S1 and S2).

Our next requirement was a set of genotypes at markers sufficiently dense to capture most causative variants. Short-read sequencing provides almost complete catalogs of genetic variants for sixteen inbred strains,[46] which are also a resource for imputing variants in the other mapping strains.[47] We carried out imputation using a hidden Markov model-based technique with proven effectiveness in inbred model organisms.[48] After imputation, we obtained genotypes on 16,767,664 markers (the imputation strategy and validation results are described in STAR Methods: imputation of genotypes). For mapping, marker sets were chosen that are polymorphic within the strains of each dataset, a number varying from 4 to 16 million SNPs segregating between the inbred strains, sufficient to identify causative variants at QTLs.[49,50]

Genetic mapping of conditioned and unconditioned fear

The phenotypic dataset we obtained is highly structured, consisting of closely related individuals (recombinant inbreds share half their genome, like full siblings) as well as distantly related individuals. Genome-wide association was carried out with GEMMA, which implements a linear mixed-model marker association test,[51,52] including a genomic relationship matrix to control for the population structure arising from the inclusion of individuals with different degrees of relatedness. We mapped each phenotype in each cohort and carried out a meta-analysis of the results using a random effects model implemented in META-SOFT.[53,54] We used Genome Reference Consortium Mouse Build 38 (GCA_000001635.2, mm10), and all coordinates in this paper refer to that build.

To assess significance, we used GCTA[55] to simulate data for each cohort and meta-analyzed the results in the same way as we did for the real datasets. From 100,000 simulations, we obtained a 5% threshold of negative logarithm (base 10) of the association p value ($\log p$) of 4.50, consistent with thresholds estimated by others using the same experimental design.[35–56] Applying this significance threshold, we identified 14 loci for FC-context, 15 for FC-cue, and 72 for EPM-open (Table S3). At a threshold corrected for testing three phenotypes ($\log p$ = 4.97) the number of loci for EPM-open fell to 60 while remaining unchanged for the other two phenotypes. Four loci were common to FC-context and FC-cue and four were common to EPM-open and FC-cue, giving 93 unique loci. The Manhattan plots in Figure 1 show all loci that exceeded the $\log p$ threshold of 4.5.

While the genetic architecture of fear-related behaviors was highly polygenic, we found evidence for a few large-effect loci, notably on chromosomes 7 and 13 for FC-cue (Figure 1A) and chromosomes 4 and 13 for FC-context (Figure 1B). More than five times as many QTLs were identified underlying EPM-open than either of the fear-conditioning phenotypes, likely reflecting higher polygenicity of the trait (Figure 1C). The size of the QTL
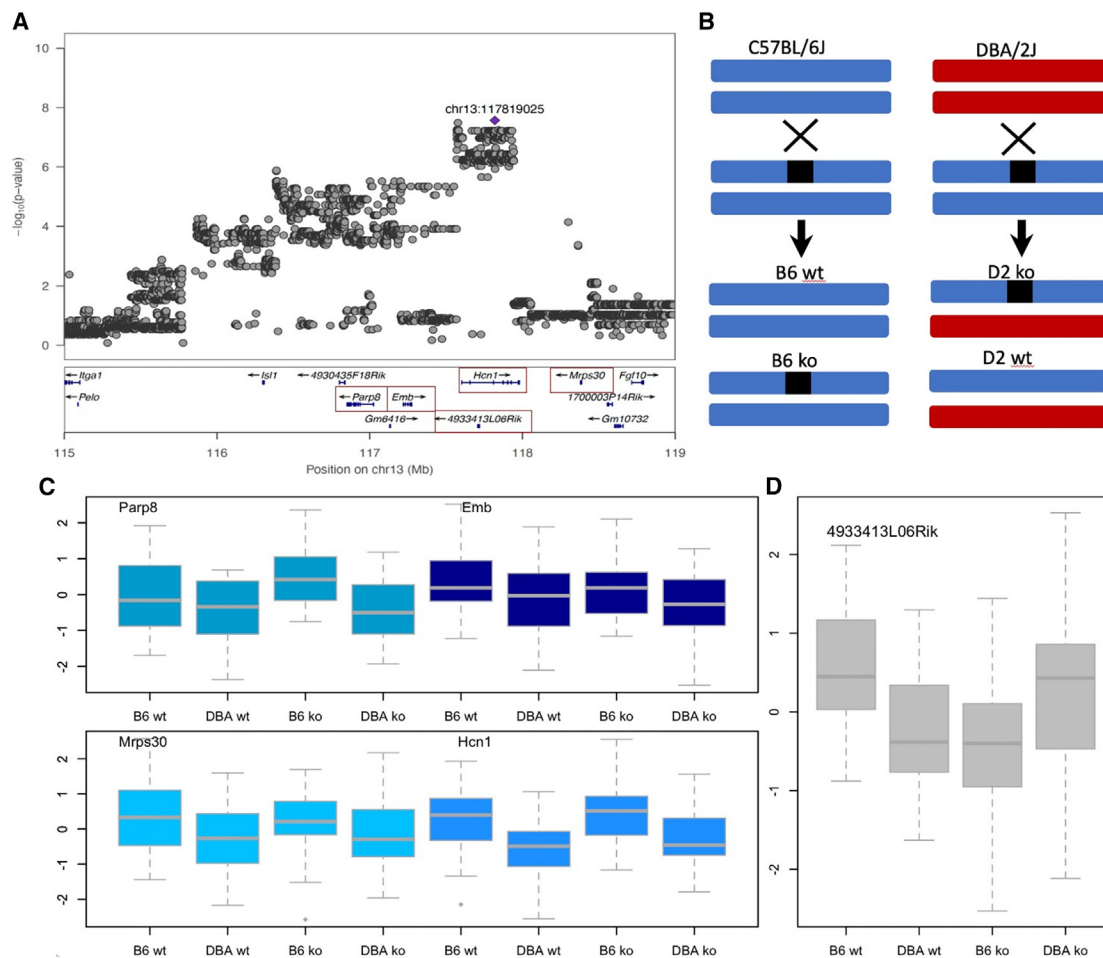
Figure 2. Quantitative complementation of five genes at a locus on chromosome 13 for cue fear conditioning

(A) QTL regional information from LocusZoom.[59] The top part shows the association results from a meta-analysis, with the position of the highest-scoring variant annotated in purple. The vertical scale is the negative logarithm (base 10) of the association p value. The bottom section gives the location and orientation of genes at the locus. A red box identifies each gene used in the quantitative complementation tests.

(B) Design of the quantitative complementation test. Black boxes indicate the knockout (KO) allele, and strain is indicated by color, where blue is C57BL/6J and red is DBA/2J. An "X" indicates a cross between the named groups above and below the X, and an arrow points to the progeny of each cross. The four groups used in the quantitative complementation test are wild-type C57BL/6J (B6 WT), heterozygote KOs (B6 KOs), an F1 from crossing DBA/2J to C57BL/6J (D2 WT), and the F1 KO by DBA/2J (D2 KO).

(C) Results of quantitative complementation testing of four annotated genes in the region. The vertical axis is the quantile normalized duration of freezing to a cue from the fear-conditioning test. The horizontal axis lists the groups of mices used. Groups are B6.WT: WT C57BL/6J; B6.KO: heterozygote KOs on C57BL/6J; D2.WT: F1 from crossing DBA/2J to C57BL/6J; D2.KO: the F1 from crossing the KO onto DBA/2J. These genes were not significant by quantitative complementation (Table 1).

(D) Results of the quantitative complementation test for the long non-coding RNA *4933413L06Rik*. The axes labels are the same as in (C). The difference between these groups yielded a significant interaction result in the quantitative complementation test (Table 1).

intervals varied considerably from 0.02 to 19.6 Mb (confidence intervals estimated by simulation[57]) with a median of 2.5 Mb, and each locus contained a median of 23 genes (range from 0 to 329; Table S3).

QC testing identifies six genes for fear-related behavior

Which of the genes at a locus is causal for the phenotype? To answer this for specific loci, we first chose a 2 Mb QTL at the end of chromosome 13 associated with FC-cue (log$p$ = 7.6), previously identified in a panel of BXD recombinant inbreds,[27] that includes a hyperpolarization-activated cyclic nucleotide-gated

channel 1 (*Hcn1*). Since pharmacological blockade of HCN1 reduces freezing, *Hcn1* has been proposed as the causal gene at this locus[27] (although deletion of *Hcn1* does not alter conditioned fear[58]). We used an exon-excision CRISPR-Cas9 strategy to knock out out all four annotated and one unannotated gene lying within the 95% confidence intervals of the QTL (Figure 2A) (we omitted the single-exon unannotated transcript *Gm6416*). We used a quantitative polymerase chain reaction to confirm that the engineered mutations altered RNA abundance. The CRISPR-Cas9 strategy and characterization of the mutants is described in STAR Methods and Tables S4 and S5.

Table 1. Quantitative complementation testing of fourteen genes at six QTLs for fear-related behavior

Phenotype	Gene	Strain p value	KO p value	Interaction p value	QTL location	N
FC-cue	Emb	5.33E−02	1.20E−01	3.73E−01	chr13:116.4–118.4	73
FC-cue	Hcn1	8.12E−02	9.93E−01	5.02E−01	chr13:116.4–118.4	100
FC-cue	Mrps30	5.67E−05	4.18E−01	8.53E−01	chr13:116.4–118.4	94
FC-cue	Parp8	2.32E−02	3.94E−01	7.00E−01	chr13:116.4–118.4	85
FC-cue	4933413L06Rik[a]	5.37E−01	6.04E−02	1.45E−03[a]	chr13:116.4–118.4	87
FC-context	Megf9	1.30E−01	3.44E−01	4.69E−01	chr4:70.1–78.2	48
FC-context	Ptprd[a]	5.15E−01	2.69E−02	1.95E−04[a]	chr4:70.1–78.2	137
FC-context	Psip1[a]	2.68E−01	2.83E−02	1.09E−03[a]	chr4:78.7–85.2	92
FC-context	Sh3gl2[a]	5.43E−02	3.09E−01	3.35E−04[a]	chr4:78.7–85.2	117
FC-context	Snapc3	8.48E−01	8.59E−01	3.00E−02	chr4:78.7–85.2	82
FC-context	Ttc39b	4.52E−01	7.28E−01	2.99E−02	chr4:78.7–85.2	75
EPM-open	Nptx2[a]	1.97E−02	2.27E−01	1.74E−03[a]	chr5:144.2–145.0	96
EPM-open	Stim2	1.85E−03	1.84E−04	1.72E−01	chr5:54.1–54.3	105
EPM-open	Lsamp[a]	2.26E−01	9.06E−02	1.17E−03[a]	chr16:41.3–41.4	79

The table shows the p values of an analysis of variance testing for an interaction between strain and knockout (KO) in the four groups of the quantitative complementation test. QTL locations are given in Mb and the name of the phenotype tested. N is the total number of animals used for the quantitative complementation test. QTL location coordinates are to mouse Genome Reference Consortium Mouse Build 38 (mm10).
[a]Results exceeding a multiple testing corrected p value of 0.0035.

Each KO was subject to a QC test (Figure 2B) to find out which gene was mediating the effect of the locus on FC-cue. Four genes tested negative (Figure 2C), while one was positive (Figure 2D), which to our surprise was an unannotated long non-coding RNA (lncRNA), *4933413L06Rik*. To interpret Figures 2C and 2D, consider that the first two groups in Figure 2B (C57BL/6J wild type [B6.WT] and DBA/2J wild type [DBA.WT]) measure a strain effect arising from a single copy of the D2 genome in the F1 animals (assuming strict additivity, the strain effect should be about half that found in inbred strain comparisons, consistent with our results). Any difference between the B6.WT and B6.KO groups is attributable to the presence of the KO.

The pattern of results in Figure 2C for the four genes tested looks identical: a strain effect can be seen but no discernable difference between groups carrying the KO and the WTs. By contrast, Figure 2D shows a different pattern. Animals with the KO do differ from their respective WTs, indicating that the KO influences the phenotype but with differences between the two strains. The B6.KO animals spend less time freezing than their WT siblings (B6.WT), while the DBA.KO group freezes more than their WT siblings (DBA.WT). In other words, the effect of the mutation depends on the strain background, which we assume to be due to a nearby QTL.

We tested this relationship between strain and KO by analysis of variance and found a significant interaction (p = 0.0015; Table 1), indicating that the effect of the QTL is mediated by the unannotated gene *4933413L06Rik*. We found no evidence of the involvement of *Hcn1*, demonstrating that QC testing can unambiguously identify genes mediating the effects of QTLs.

We next tackled the most significant region of association for FC-context, a 15-Mb region on chromosome 4 (between 70 and 85). There were two QTLs here (70–78 and 79–85 Mb; Figure 3), together containing 46 genes. To narrow the choice of genes, we tested genes close to the most highly associated markers and

with confirmed gene expression in the hippocampus and amygdala (from published sources[60–67]). At the first locus, the interaction p value of *Ptprd* exceeded a multiple correction testing threshold (p < 0.0036 for testing 14 genes listed in Table 1), while at the second two genes, *Psip1* and *Sh3gl3*, exceeded the threshold (results shown in Figure 3 and Table 1).

Finally, we chose three loci contributing to variation in EPM-open behavior (Figure 4). The first, on chromosome 16, had a highly significant association (log$p$ = 9.48) and lies in an intron of a cell adhesion molecule, *Lsamp* (limbic system-associated membrane protein), whose deletion is known to alter behavior in the EPM.[68,69] We found a significant interaction (p = 0.001; Table 1), indicating that the effect of the QTL is mediated by the *Lsamp* gene. We tested *Stim2* and *Nptx2* at two other loci using the same CRISPR-Cas9 exon deletion approach. While the QC test confirmed the candidacy of *Nptx2,* it was negative for *Stim2*. Table 1 summarizes the results of the QC tests for all genes at the six loci we examined.

Strain differences in gene expression, open chromatin, and methylation are concentrated in excitatory hippocampal neurons

One hypothesis about how QTLs act is that they alter gene expression, which in our case would manifest as a difference in the abundance of transcripts from C57BL/6J and DBA/2J genomes in relevant cell types. With six genes in hand, we set out to test this assumption. We generated single-nucleus RNA-sequencing (snRNA-seq) datasets in C57BL/6J and DBA/2J animals from the ventral hippocampus and amygdala. We identified 17 cell types in the ventral hippocampus and 22 in the amygdala with two replicates per strain per region (Figure 5, joint uniform manifold approximation and projection). The clusters included excitatory (glutamatergic) and inhibitory (GABAergic) neurons, as well as several types of non-neuronal cells that
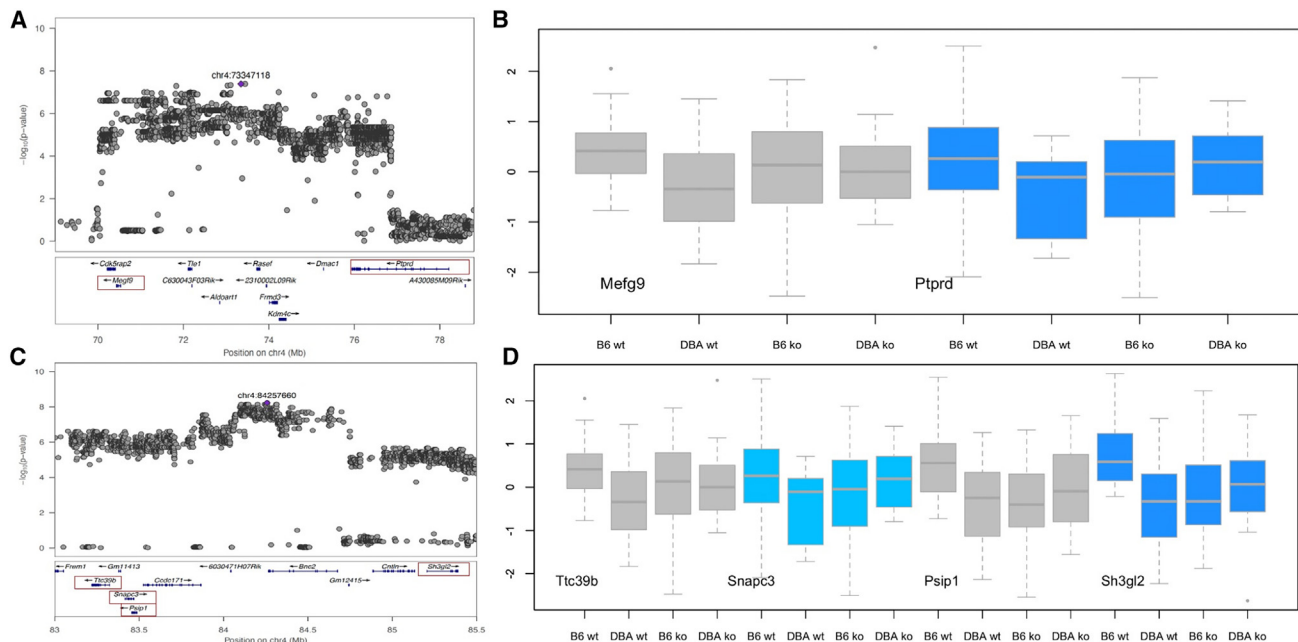
Figure 3. Quantitative complementation of four genes at two QTLs on chromosome 4 for contextual fear conditioning
(A and C) QTL regional information from LocusZoom.[59] The top part shows the association results from a meta-analysis, with the position of the highest-scoring variant annotated in purple. The vertical scale is the negative logarithm (base 10) of the association *p* value. The bottom section gives the location and orientation of genes at the locus. A red box identifies each gene used in the quantitative complementation tests.
(B and D) Results of quantitative complementation testing of six annotated genes. The vertical axis is the quantile normalized duration of freezing to the context from the fear-conditioning test. The horizontal axis lists the groups of mice used. Groups are B6.WT: WT C57BL/6J; B6.KO: heterozygote KOs on C57BL/6J; D2.WT: F1 from crossing DBA/2J to C57BL/6J; D2.KO: the F1 from crossing the KO onto DBA/2J. Genes significant by quantitative complementation are shown in gray (results in Table 1).

were annotated based on known marker genes. We define individual neuronal cell types based on neurotransmitter expression and region or top marker gene (for example, Exc-DG in the ventral hippocampus refers to excitatory cells in the dentate gyrus, and Exc-Tafa1 in the amygdala refers to excitatory cells marked by the gene *Tafa1*), and we define neuronal cell class as either excitatory or inhibitory through combining all excitatory or all inhibitory cell types, respectively (one amygdala neuronal type was excluded from both cell classes due to the expression of both excitatory and inhibitory markers). Non-neuronal cell types were not further defined due to an enrichment step for neuronal nuclei during sample processing limiting the number of non-neuronal nuclei captured.

Given that QTL action is believed to have its effect on transcription through the alteration of the sequence at regulatory regions, we also generated single-nucleus data for CpG methylation[70] and from a single-nucleus assay of transposase-accessible chromatin (snATAC-seq).[71] Both epigenetic modalities can be used to identify regulatory elements, such as promoters and enhancers.[72] Cell-type clusters generated from snRNA profiles were propagated to snATAC and methylation datasets through joint embedding (Figure 5). We confirmed that cell types were integrated by modality (Figures 5A and 5D), that there was no obvious strain bias for cell types (Figures 5B and 5E), and that cell types were well defined (Figures 5C and 5F). Importantly for interpreting our analyses, the three epigenetic datasets were

obtained independently from different animals, with two independent replicates per modality.

Five out of six genes showed significant differences in expression between C57BL/6J and DBA/2J (significance defined as exceeding a 10% *p* value [log*p* > 1.0], adjusted for the total number of transcripts tested, from DEseq2[73] output; negative log2 fold change [log2FC] indicates higher expression in B6): *4933413L06Rik* (in eleven cell types; median log2FC = −0.74, range = −1.63 to −0.53), *Lsamp* (in eleven cell types; median log2FCc = −0.21, range = −0.78 to 1.1), *Psip1* (in five cell types; median log2FC = 0.41, range = 0.30 to 0.49), Nptx2 (in one cell type; log2FC = 1.82), and *Ptprd* (in eight cell types; median log2FC = −0.31, range = −1.24. to 1.85). Of the 36 cell types exhibiting differential expression for these genes, 31 were within the hippocampus. Different hippocampal cell types showed different degrees of overlap for differential gene expression of genes; for example, four of the five genes were differentially expressed within Exc-CA1-Galntl6 cells, while only *4933413L06Rik* was differentially expressed within Exc-CA1-Camk2d cells. We noted that 22 of the 31 significant differences in the hippocampus and three out of five significant differences in the amygdala occurred in cell types categorized as excitatory neurons. Results of the DESeq2 analyses are given in Table S6.

We asked if the pattern of gene expression also held for snATAC-seq and methylation profiles, namely showing more strain differences in the hippocampus with an enrichment in excitatory
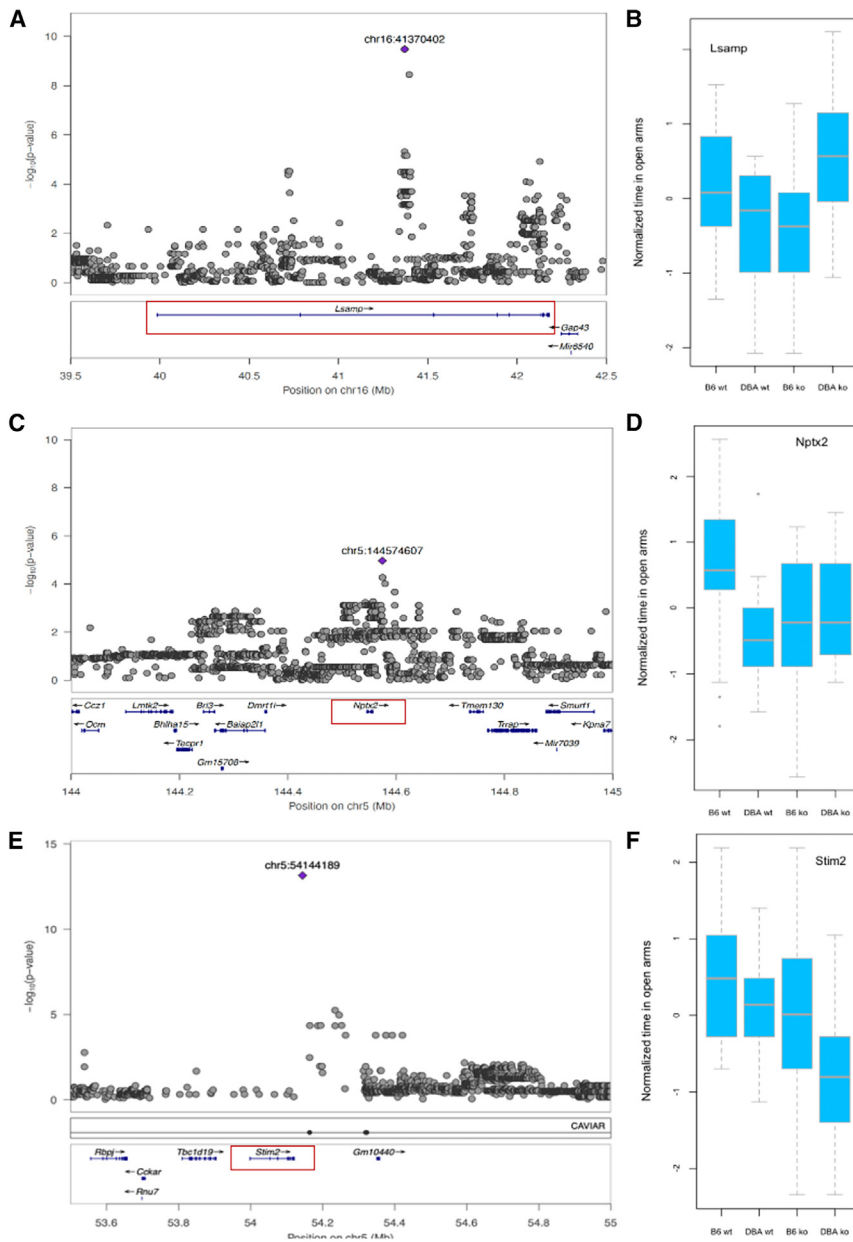
Figure 4. Quantitative complementation of three genes at three QTLs for the number of entries into the open arms of the EPM

(A, C, and E) QTL regional information from LocusZoom.[59] The top part shows the association results from a meta-analysis, with the position of the highest-scoring variant annotated in purple. The vertical scale is the negative logarithm (base 10) of the association p value. The bottom section gives the location and orientation of genes at the locus. A red box identifies each gene used in the quantitative complementation tests.

(B, D, and F) Results of quantitative complementation testing. The vertical axis is the quantile normalized duration of the number of entries into the open arms of the elevated plus maze. The horizontal axis lists the groups of mice used. Groups are B6.WT: WT C57BL/6J; B6.KO: heterozygote KOs on C57BL/6J; D2.WT: F1 from crossing DBA/2J to C57BL/6J; D2.KO: the F1 from crossing the KO onto DBA/2J.

presented in Figure 6. First, there were more strain differences in the hippocampus than amygdala, as reflected in the greater number of dots compared to crosses. Second, at each locus, the strain differences were found primarily in excitatory neurons, in both the hippocampal and amygdala, as shown by the preponderance of red. Third, the pattern of strain differences for each modality varied between loci and genes, providing no unequivocal location or molecular signature to identify causal variants. The *Ptprd* locus (Figure 6A) contained a concentration of methylation, ATAC sites, and sequence differences at the 3′ end of the gene, suggesting a location for one or more causal variants here. At the *Psip1* and *Sh3gl2* locus (Figure 6B), strain differences were spread across the region with no indication of which might be relevant. The QTLs containing *4933413L06Rik* (Figure 6C) and *Nptx2* (Figure 6D) included a concentration of strain differences in methylation sites around the genes but with no obvious candidates for causative variants. One possible exception was the single ATAC site that exceeded a corrected significance threshold ($\log p = 6$) in an intron of the *Lsamp* gene (Figure 6E) coinciding with a 2-kb deletion in DBA/2J. The function of this site and the consequences of its deletion are not known.

The apparent enrichment of genetically mediated variation in excitatory neurons at the five QTLs containing the causal genes led us to examine whether the same was true for all the QTLs we had identified. We compared gene expression and epigenetic variation at 93 QTLs with the rest of the genome, expecting that any enrichment would be confined to, or more prominent at, the QTLs. Surprisingly, although the QTLs occupy about 0.01% of the genome, the percentage of significantly different

neurons. To do this, we made an inventory of variable snATAC-seq and methylation sites. We counted differential ATAC sites (using a 5% threshold from adjusted p values derived from DESeq2[73]) that contained sequence variants under the assumption that differences at these sites were more likely genetic in origin than those without such differences (more than 90% of the significantly different ATAC sites contain a sequence variant compared to 35% of non-variable sites). For the methylation data, we counted the number of fully methylated CpG sites in each cell type and divided them into those with and without mutations that disrupted methylation.

Figure 6 plots differential methylation and ATAC sites in the hippocampus and amygdala at the five QTLs where we identified causal genes. Three general observations arose from the data
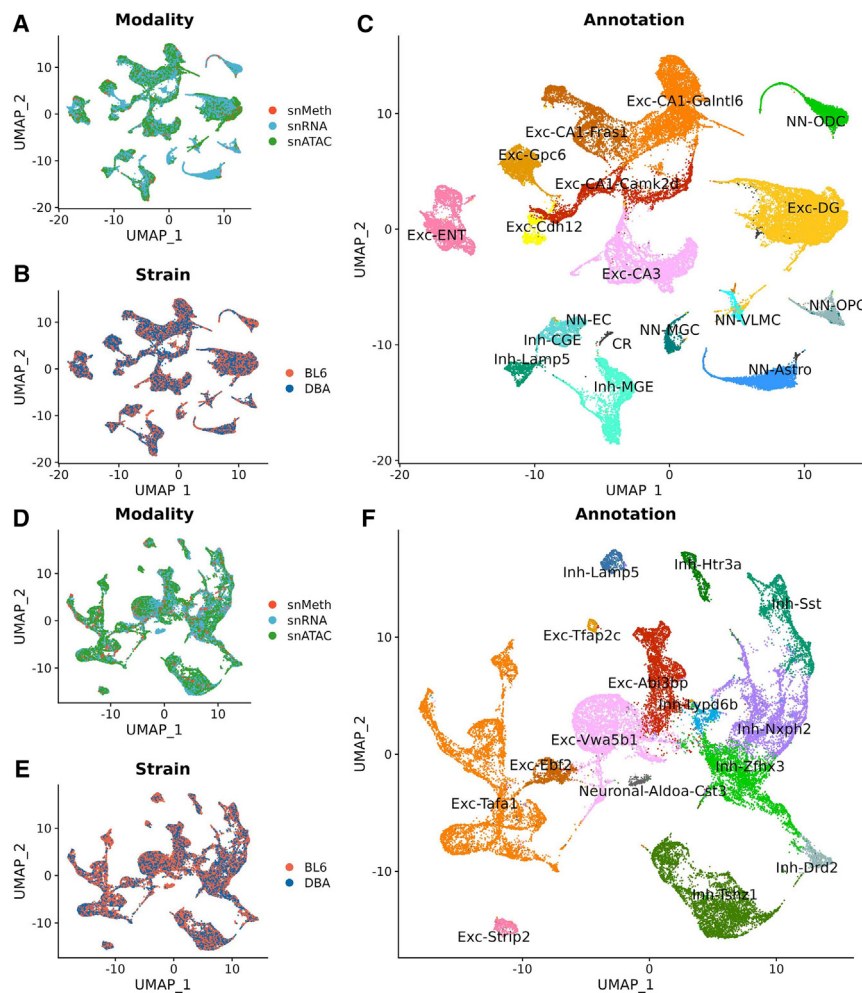
A Modality

B Strain

C Annotation

D Modality

E Strain

F Annotation

and above the contribution of sequence coverage. A generalized linear model to predict differences also showed that sequence coverage does not account for the differences between excitatory and inhibitory neurons (Table S10).

Second, the inclusion of more excitatory cell types than inhibitory types could bias findings (eight excitatory cell types compared to three inhibitory in the hippocampus) because the addition of extra cell types increases the chances of finding variant sites. Against this, we note that in the amygdala, there were more inhibitory than excitatory cell types (eight versus six). We ran a test of this hypothesis, by comparing the contribution of class (excitatory and inhibitory) to cell type, considering that cell type was completely nested within class. We resorted to a Bayesian analysis, which revealed a significant effect of class (the 95% confidence intervals do not overlap zero) (Table S11).

Is the enrichment in excitatory cells a peculiarity of the difference between C57BL/6J and DBA/2J? We answered this question for the hippocampus using methylation data from six other strains. Using CAST/EiJ as an outgroup, we compared the number of mutations in CpG sites at excitatory and inhibitory neurons in the ventral hippocampus. Table S12 shows that for each strain, compared to CAST/EiJ, the proportion of mutated CpG sites was higher in excitatory than inhibitory neurons, supporting our finding that at least for methylation, alterations in functional elements directly attributable to genetic variation were enriched in excitatory neurons compared to other cell types. Together, these results suggest a model whereby genetic effects act on specific hubs of circuits/cell types.

DISCUSSION

We have established the feasibility of combining mapping with QC testing for gene identification, breaking open a bottleneck in the genetic dissection of complex traits in mice, and provided a set of six genes for further mechanistic understanding of fear-related behavior. Unexpectedly, genetically mediated variation in three independent molecular analyses, methylation, snRNA-seq, and snATAC-seq, was found to occur preferentially in

transcripts (again defined as exceeding a 5% threshold from adjusted p values derived from DESeq2[73]) in QTL regions was indistinguishable from the percentage of significantly different transcripts in the genome (Figure 6F), a finding replicated for methylation and snATAC-seq data (Tables S7 and S8). In other words, there was no enrichment in QTLs for genetically mediated variation in excitatory neurons; all regions of the genome contribute to this phenomenon.

Is the enrichment of genetic variants in excitatory neurons significant? It certainly seems so, but at least two confounds could produce this result. For the snATAC-seq and snRNA-seq data, identification of significant strain differences is more likely with higher read coverage, and for methylation, the more sites we identify, the higher the likelihood that some will coincide with a sequence variant. To assess the contribution of sequence coverage, we compared a null model, in which sequence coverage predicted the number of differentially expressed genes, ATAC peaks, or methylation sites with mutations, to one that additionally included cell type and found highly significant improvements in fit (all p values $< 2.2E-16$; Table S9), demonstrating that cell type was an important contributor, over

Figure 6. ATAC-seq and methylation data at five QTLs in the ventral hippocampus and amygdala

(A–E) Data from the hippocampus are marked by dots (•) and data from the amygdala by crosses (+). In each image, the lowest row shows the distribution of genetic variants (black). The next two tracks, immediately below the genes and indicated by the blue background, show the location of methylation sites that coincide with a sequence variant and are thus present in only one of the two strains. These sites are colored according to the class of cell type in which they occur: red for excitatory neurons, blue for inhibitory neurons, and gray for non-neuronal cell types. Above the methylation tracks are shown ATAC sites, which differ significantly between the strains. The vertical axis shows the absolute value of log2 fold change for these ATAC sites. Sites are again colored according to the class of cell type in which they occur using the same color scheme as for methylation. The vertical positioning of the genes is only for ease of plotting and carries no meaning.

(F) Comparison of the percentage of significantly different RNA species in QTL regions and in the genome for the hippocampus. The vertical axis is the percentage of transcripts that are significantly different between the two strains, and the horizontal axis lists the cell types. Data from QTL intervals are indicated by dots colored according to class: excitatory (red), inhibitory (blue), and non-neuronal (gray). Data from the entire genome are indicated by black crosses.

excitatory neurons and to be enriched in the hippocampus compared to the amygdala. These observations demonstrate the possibility of moving quickly from locus to gene, identify unexplored biology underlying fear-related behavior, and raise questions about expected relationships between genetic and functional variation.

Our findings highlight the power of unbiased genetic examination of the biological basis of behavioral variation. At a locus on chromosome 13, we made the unexpected discovery that an lncRNA (*4933413L06Rik*) is involved in cue fear conditioning. Little is known about *4933413L06Rik* (one study found it to be differentially expressed during development of the auditory forebrain[74]). Our finding opens the possibility for clarifying the function of this lncRNA in fear-related behavior. Two other causal genes (*Psip1*, *Sh3gl2*) have also never been studied in the context of fear-related behaviors. We note that of the five genes with known functions, four (*Lsamp*, *Ptprd*, *Nptx2*, and *Sh3gl2*) are implicated in synapse development or function.[75–79] Ptprd belongs to the type IIA receptor-type protein tyrosine phosphatase family of phosphatases, involved in synaptic formation and structure during development and neurogenesis.[76] Lsamp is a cell surface adhesion molecule

that is involved in neuritogenesis and axon guidance (and is also implicated in the maturation of serotonergic[80] and thalamocortical circuits[81]). Nptx2 is a secreted glycoprotein that localizes to both pre- and post-synaptic compartments of excitatory synapses containing AMPA receptors and is involved with synaptogenesis[82] and adult neurogenesis.[83] *Sh3gl2* (endophilin1), a cytoplasmic Src homology 3 domain-containing protein,[84] localizes to presynaptic nerve terminals, where it functions in synaptic vesicle endocytosis[85] and the regulation of exocytosis.[86] The significance of these functional observations is difficult to assess, but it at least suggests that variation in fear-related behavior in part originates in synaptic development.

The QC test could serve as a gold standard for gene identification following QTL mapping in inbred mice. Following mapping, the construction of KOs is relatively straightforward, and the test requires a simple breeding protocol. We recommend powering the QC tests based on results from the mapping experiment (the effect size of the locus in the mapping population will be lower than that in QC test[87]), but note that our failure to detect a candidate gene at a locus on chromosome 5 could be due to low power or because we tested the wrong gene.

Our instantiation of the QC test is not the only one; alternative designs are possible. For example, in an experiment to test the candidacy of a gene at a QTL for resistance to obesity in mice, a QC test was constructed from a KO, a subcongenic containing the QTL, and their corresponding background strains (a cross giving rise to four genotypes on a uniform genetic background).[88] However, it is essential to use KOs on an isogenic background so as to avoid the complication of the effect of additional QTLs that may be present on the non-isogenic DNA.

Interpretation of the QC results is subject to some qualifications. First, while a positive QC test result reveals a gene through which a QTL has its effect, it does not necessarily mean that the QTL is the one containing the candidate gene. The QC test will detect the effect of any QTL that requires the gene to be present. Typically, that QTL will be the one local to the gene tested, but that assumption is not essential for the functioning of the QC test. Second, the QC test makes no assumptions about how the QTL and KO interact. Does this matter? It may, because in the QC test, non-additive interactions are typically easier to detect than additive ones. Under an additive model, the KO removes the effect of one of the QTLs so that the phenotypic effect is reduced by the allelic effect of that QTL. In non-additive models, the presence of the KO could reduce one QTL effect to zero (recessive effect) or increase it, potentially in a multiplicative fashion. In these cases, the effect of the interaction is to augment the allelic effect over that of the additive interaction. We have some evidence that non-additive interactions predominate in our results.

QC tests results from four genes (*Lsamp*, *Ptprd*, *4933413L06Rik*, and *Psip1*) are consistent with a non-additive interaction between QTL and KO. In each case, the phenotype of the KO on the hybrid background is larger than either the WT DBA/2J or the KO on the C57BL/6J (Figures 2, 3, and 4). One interpretation is that non-additivity is common. Another interpretation is that we failed to detect additive interactions because non-additivity is easier to detect: the larger effect attributable to the interaction confers greater power for the QC test. This may contribute to false negative findings, but it does not undermine the conclusion that the effect of the QTL is mediated by the gene. Under both additive and non-additive models, a significant result means that the effect of the QTL requires the gene.

One tantalizing corollary emerging from the analysis of gene causality in fear-related behaviors is that genetic variation may act preferentially in excitatory, rather than inhibitory, neurons. We note that any patterns of strain differences could not be attributed solely to coverage, as even downsampling our RNA-seq and ATAC-seq data to as low as 25% of the total unique molecular identifiers still resulted in substantial detection of significant strain differences (see https://dx.doi.org/10.6084/m9.figshare.25521304). We had expected that the pattern of strain differences might point to the involvement of a particular cell type in one region of the brain. Instead of finding cell-type enrichment, we observed that strain differences in three different modalities, snRNA-seq, methylation, and snATAC-seq, were more prevalent in excitatory than inhibitory neurons, particularly in the hippocampus compared to the amygdala. Moreover, we found this enrichment pattern to be true not just for the QTL re-gions but for the entire genome. There was little evidence of strain differences in non-neuronal tissues, although we can be less confident in this assertion because our sample was enriched for neuronal cells and may not be representative of non-neuronal variation.

What might explain this finding? One possibility is that it is specific to a comparison between C57BL/6J and DBA/2J. We think that this is unlikely and provide some evidence against this idea by running a similar analysis for methylation data in other strain comparisons, though we have not extended this observation to other modalities. Alternatively, the finding represents a preference for genetic effects in excitatory neurons. Why might this be so?

The idea that genetic effects operate preferentially in excitatory neurons fits with a neuronal circuit model where inhibitory neurons sculpt behaviors driven by excitatory neurons. Excitatory neurons are extremely diverse, resulting in high-dimensional and sparse coding,[89] consistent with the expectation that such an architecture permits highly efficient information transfer.[90] Consequently, encoding within excitatory networks cannot be predicted from their transcriptome alone. In contrast, activity within inhibitory neuronal networks is lower dimensional, with correlations between inhibitory cell types determined primarily by cell type, so that cells belonging to a single transcriptomic class are highly correlated.[91–93] In this model, genetic variation is more permissible in excitatory neuronal networks than inhibitory, suggesting that disturbances of inhibitory networks are more likely to be pathological. If this interpretation is correct, then identifying genetic effects that disturb function at a circuit level may be more fruitful than looking for cell-type-specific genetic effects.

Limitations of the study

Our results are subject to some limitations. First, the results from the meta-analysis have not been replicated, so it is possible that some of the loci may be false positive. This may explain why the QC test was negative for *Stim2* on chromosome 5. Second, some of the negative QC test results may be due to relatively low power to detect additive effects compared to non-additive effects. Third, we did not test every expressed transcript at every QTL. For instance, it is possible that single-exon unannotated transcripts (e.g., *Gm6416*, which we did not test at the chromosome 13 locus) might also contribute. However, the failure to detect the involvement of additional genes does not mitigate the main result of our experiment, namely, that the QC test can be used in a systematic fashion to identify genes mediating the QTL effect.

STAR★METHODS

Detailed methods are provided in the online version of this paper and include the following:

- KEY RESOURCES TABLE
- RESOURCE AVAILABILITY
  - Lead contact
  - Materials availability
  - Data and code availability
- EXPERIMENTAL MODEL AND STUDY PARTICIPANT DETAILS

- ○ Mouse strains
- ● METHOD DETAILS
  - ○ Mouse phenotyping and mapping
  - ○ Harmonizing phenotyping data for meta-analysis
  - ○ Behavioral phenotyping
  - ○ Behavioral tests
  - ○ Elevated plus maze
  - ○ Fear-conditioning
  - ○ Behavioral analysis
  - ○ Genotyping
  - ○ Imputation of genotypes
  - ○ Genetic mapping
  - ○ Significance threshold for the genome-wide association studies
  - ○ Generating knockout animals for QC testing
  - ○ Quantitative polymerase chain reactions
  - ○ Quantitative complementation testing
  - ○ Ventral hippocampus microdissections
  - ○ Amygdala microdissections
  - ○ Generating snmC-seq2 libraries
  - ○ Generating snRNA-seq libraries
  - ○ Generating snATAC-seq libraries
- ● QUANTIFICATION AND STATISTICAL ANALYSIS
  - ○ Single-nucleus RNA sequencing data quality control and pre-processing
  - ○ Single-nucleus ATAC sequencing data quality control and pre-processing
  - ○ Single-nucleus methylation data quality control and pre-processing
  - ○ Single-nucleus RNA sequencing data integration, clustering and annotation
  - ○ Single-nucleus ATAC sequencing data integration, clustering and annotation
  - ○ Single-cell methylation data integration, clustering and annotation
  - ○ Co-embedding of single-nucleus RNA, single-nucleus ATAC, and single-nucleus methylation sequencing data
  - ○ Cell-type specific differential test for single-nucleus ATAC and single-nucleus RNA
  - ○ Testing class and cell type effects on strain differences

SUPPLEMENTAL INFORMATION

Supplemental information can be found online at https://doi.org/10.1016/j.xgen.2024.100545.

AUTHOR CONTRIBUTIONS

R.C. performed the mouse breeding and behavioral experiments. C.L. performed the single-cell methylation analyses, data from which were processed by M.G.H. and Z.C. P.B.C. performed the snRNA and snATAC analyses, with data processing by Z.C. J.F., P.B.C., and D.C.S. analyzed data from the single-cell experiments. J.F. and N.L. analyzed the mouse mapping data. J.M. provided statistical support. J.F. and P.B.C. designed the study. P.B.C., J.F., and E.M. co-wrote the manuscript, which was subsequently reviewed and edited by the rest of the authors.

DECLARATION OF INTERESTS

The authors declare no competing interests.

REFERENCES

1. Abdellaoui, A., Yengo, L., Verweij, K.J.H., and Visscher, P.M. (2023). 15 years of GWAS discovery: Realizing the promise. Am. J. Hum. Genet. *110*, 179–194.

2. Flint, J., and Eskin, E. (2012). Genome-wide association studies in mice. Nat. Rev. Genet. *13*, 807–817.

3. Mackay, T.F. (2001). Quantitative trait loci in Drosophila. Nat. Rev. Genet. *2*, 11–20.

4. Yalcin, B., Willis-Owen, S.A.G., Fullerton, J., Meesaq, A., Deacon, R.M., Rawlins, J.N.P., Copley, R.R., Morris, A.P., Flint, J., and Mott, R. (2004). Genetic dissection of a behavioral quantitative trait locus shows that Rgs2 modulates anxiety in mice. Nat. Genet. *36*, 1197–1202.

5. Mali, P., Yang, L., Esvelt, K.M., Aach, J., Guell, M., DiCarlo, J.E., Norville, J.E., and Church, G.M. (2013). RNA-guided human genome engineering via Cas9. Science *339*, 823–826.

6. Wang, H., Yang, H., Shivalila, C.S., Dawlaty, M.M., Cheng, A.W., Zhang, F., and Jaenisch, R. (2013). One-step generation of mice carrying mutations in multiple genes by CRISPR/Cas-mediated genome engineering. Cell *153*, 910–918.

7. Bannerman, D.M., Rawlins, J.N.P., McHugh, S.B., Deacon, R.M.J., Yee, B.K., Bast, T., Zhang, W.N., Pothuizen, H.H.J., and Feldon, J. (2004). Regional dissociations within the hippocampus–memory and anxiety. Neurosci. Biobehav. Rev. *28*, 273–283.

8. Tovote, P., Fadok, J.P., and Lüthi, A. (2015). Neuronal circuits for fear and anxiety. Nat. Rev. Neurosci. *16*, 317–331.

9. Xu, C., Krabbe, S., Gründemann, J., Botta, P., Fadok, J.P., Osakada, F., Saur, D., Grewe, B.F., Schnitzer, M.J., Callaway, E.M., and Lüthi, A. (2016). Distinct Hippocampal Pathways Mediate Dissociable Roles of Context in Memory Retrieval. Cell *167*, 961–972.e16.

10. Wolff, S.B.E., Gründemann, J., Tovote, P., Krabbe, S., Jacobson, G.A., Müller, C., Herry, C., Ehrlich, I., Friedrich, R.W., Letzkus, J.J., and Lüthi, A. (2014). Amygdala interneuron subtypes control fear learning through disinhibition. Nature *509*, 453–458.

11. Felix-Ortiz, A.C., Beyeler, A., Seo, C., Leppla, C.A., Wildes, C.P., and Tye, K.M. (2013). BLA to vHPC inputs modulate anxiety-related behaviors. Neuron *79*, 658–664.

12. Tye, K.M., Prakash, R., Kim, S.Y., Fenno, L.E., Grosenick, L., Zarabi, H., Thompson, K.R., Gradinaru, V., Ramakrishnan, C., and Deisseroth, K. (2011). Amygdala circuitry mediating reversible and bidirectional control of anxiety. Nature *471*, 358–362.

13. Davis, M. (1992). The role of the amygdala in fear and anxiety. Annu. Rev. Neurosci. *15*, 353–375.

14. LeDoux, J.E. (2000). Emotion circuits in the brain. Annu. Rev. Neurosci. *23*, 155–184.

15. Maren, S. (2001). Neurobiology of Pavlovian fear conditioning. Annu. Rev. Neurosci. *24*, 897–931.

16. Bailey, J.S., Grabowski-Boase, L., Steffy, B.M., Wiltshire, T., Churchill, G.A., and Tarantino, L.M. (2008). Identification of quantitative trait loci for locomotor activation and anxiety using closely related inbred strains. Genes Brain Behav. *7*, 761–769.

17. Bolivar, V.J., Caldarone, B.J., Reilly, A.A., and Flaherty, L. (2000). Habituation of activity in an open field: A survey of inbred strains and F1 hybrids. Behav. Genet. *30*, 285–293.

18. Bolivar, V.J., Pooler, O., and Flaherty, L. (2001). Inbred strain variation in contextual and cued fear conditioning behavior. Mamm. Genome *12*, 651–656.

19. Bothe, G.W.M., Bolivar, V.J., Vedder, M.J., and Geistfeld, J.G. (2005). Behavioral differences among fourteen inbred mouse strains commonly used as disease models. Comp. Med. *55*, 326–334.

20. Brigman, J.L., Mathur, P., Lu, L., Williams, R.W., and Holmes, A. (2009). Genetic relationship between anxiety-related and fear-related behaviors in BXD recombinant inbred mice. Behav. Pharmacol. *20*, 204–209.

21. Carhuatanta, K.A.K., Shea, C.J.A., Herman, J.P., and Jankord, R. (2014). Unique genetic loci identified for emotional behavior in control and chronic stress conditions. Front. Behav. Neurosci. *8*, 341.

22. Cook, M.N., Williams, R.W., and Flaherty, L. (2001). Anxiety-related behaviors in the elevated zero-maze are affected by genetic factors and retinal degeneration. Behav. Neurosci. *115*, 468–476.

23. Delprato, A., Bonheur, B., Algéo, M.P., Rosay, P., Lu, L., Williams, R.W., and Crusio, W.E. (2015). Systems genetic analysis of hippocampal neuroanatomy and spatial learning in mice. Genes Brain Behav. *14*, 591–606.

24. Geuther, B.Q., Deats, S.P., Fox, K.J., Murray, S.A., Braun, R.E., White, J.K., Chesler, E.J., Lutz, C.M., and Kumar, V. (2019). Robust mouse tracking in complex environments using neural networks. Commun. Biol. *2*, 124.

25. Gubner, N.R., Wilhelm, C.J., Phillips, T.J., and Mitchell, S.H. (2010). Strain differences in behavioral inhibition in a Go/No-go task demonstrated using 15 inbred mouse strains. Alcohol Clin. Exp. Res. *34*, 1353–1362.

26. Keum, S., Park, J., Kim, A., Park, J., Kim, K.K., Jeong, J., and Shin, H.S. (2016). Variability in empathic fear response among 11 inbred strains of mice. Genes Brain Behav. *15*, 231–242.

27. Knoll, A.T., Halladay, L.R., Holmes, A.J., and Levitt, P. (2016). Quantitative Trait Loci and a Novel Genetic Candidate for Fear Learning. J. Neurosci. *36*, 6258–6268.

28. Koide, T., Moriwaki, K., Ikeda, K., Niki, H., and Shiroishi, T. (2000). Multi-phenotype behavioral characterization of inbred strains derived from wild stocks of Mus musculus. Mamm. Genome *11*, 664–670.

29. Lad, H.V., Liu, L., Paya-Cano, J.L., Parsons, M.J., Kember, R., Fernandes, C., and Schalkwyk, L.C. (2010). Behavioural battery testing: evaluation and behavioural outcomes in 8 inbred mouse strains. Physiol. Behav. *99*, 301–316.

30. Loos, M., van der Sluis, S., Bochdanovits, Z., van Zutphen, I.J., Pattij, T., Stiedl, O., Neuro-BSIK Mouse Phenomics consortium; Smit, A.B., and Spijker, S. (2009). Activity and impulsive action are controlled by different genetic and environmental factors. Genes Brain Behav. *8*, 817–828.

31. Miller, B.H., Schultz, L.E., Gulati, A., Su, A.I., and Pletcher, M.T. (2010). Phenotypic characterization of a genetically diverse panel of mice for behavioral despair and anxiety. PLoS One *5*, e14458.

32. Milner, L.C., and Crabbe, J.C. (2008). Three murine anxiety models: results from multiple inbred strain comparisons. Genes Brain Behav. *7*, 496–505.

33. O'Leary, T.P., Gunn, R.K., and Brown, R.E. (2013). What are we measuring when we test strain differences in anxiety in mice? Behav. Genet. *43*, 34–50.

34. Owen, E.H., Christensen, S.C., Paylor, R., and Wehner, J.M. (1997). Identification of quantitative trait loci involved in contextual and auditory-cued fear conditioning in BXD recombinant inbred strains. Behav. Neurosci. *111*, 292–300.

35. Park, C.C., Gale, G.D., de Jong, S., Ghazalpour, A., Bennett, B.J., Farber, C.R., Langfelder, P., Lin, A., Khan, A.H., Eskin, E., et al. (2011). Gene networks associated with conditional fear in mice identified using a systems genetics approach. BMC Syst. Biol. *5*, 43.

36. Philip, V.M., Duvvuru, S., Gomero, B., Ansah, T.A., Blaha, C.D., Cook, M.N., Hamre, K.M., Lariviere, W.R., Matthews, D.B., Mittleman, G.,

et al. (2010). High-throughput behavioral phenotyping in the expanded panel of BXD recombinant inbred strains. Genes Brain Behav. *9*, 129–159.

37. Philip, V.M., Sokoloff, G., Ackert-Bicknell, C.L., Striz, M., Branstetter, L., Beckmann, M.A., Spence, J.S., Jackson, B.L., Galloway, L.D., Barker, P., et al. (2011). Genetic analysis in the Collaborative Cross breeding population. Genome Res. *21*, 1223–1238.

38. Ponder, C.A., Munoz, M., Gilliam, T.C., and Palmer, A.A. (2007). Genetic architecture of fear conditioning in chromosome substitution strains: relationship to measures of innate (unlearned) anxiety-like behavior. Mamm. Genome *18*, 221–228.

39. Sittig, L.J., Carbonetto, P., Engel, K.A., Krauss, K.S., Barrios-Camacho, C.M., and Palmer, A.A. (2016). Genetic Background Limits Generalizability of Genotype-Phenotype Relationships. Neuron *91*, 1253–1259.

40. Takahashi, A., Kato, K., Makino, J., Shiroishi, T., and Koide, T. (2006). Multivariate analysis of temporal descriptions of open-field behavior in wild-derived mouse strains. Behav. Genet. *36*, 763–774.

41. Trullas, R., and Skolnick, P. (1993). Differences In Fear Motivated Behaviors Among Inbred Mouse Strains. Psychopharmacology *111*, 323–331.

42. Wahlsten, D., Metten, P., and Crabbe, J.C. (2003). Survey of 21 inbred mouse strains in two laboratories reveals that BTBR T/+ tf/tf has severely reduced hippocampal commissure and absent corpus callosum. Brain Res. *971*, 47–54.

43. Wiltshire, T., Ervin, R.B., Duan, H., Bogue, M.A., Zamboni, W.C., Cook, S., Chung, W., Zou, F., and Tarantino, L.M. (2015). Initial locomotor sensitivity to cocaine varies widely among inbred mouse strains. Genes Brain Behav. *14*, 271–280.

44. Yang, R.J., Mozhui, K., Karlsson, R.M., Cameron, H.A., Williams, R.W., and Holmes, A. (2008). Variation in mouse basolateral amygdala volume is associated with differences in stress reactivity and fear learning. Neuropsychopharmacology *33*, 2595–2604.

45. de Mooij-van Malsen, J.G., Yu, K.L., Veldman, H., Oppelaar, H., van den Berg, L.H., Olivier, B., and Kas, M.J.H. (2009). Variations in ventral root axon morphology and locomotor behavior components across different inbred strains of mice. Neuroscience *164*, 1477–1483.

46. Lilue, J., Doran, A.G., Fiddes, I.T., Abrudan, M., Armstrong, J., Bennett, R., Chow, W., Collins, J., Collins, S., Czechanski, A., et al. (2018). Sixteen diverse laboratory mouse reference genomes define strain-specific haplotypes and novel functional loci. Nat. Genet. *50*, 1574–1583.

47. Marchini, J., and Howie, B. (2010). Genotype imputation for genome-wide association studies. Nat. Rev. Genet. *11*, 499–511.

48. Kang, H.M., Zaitlen, N.A., and Eskin, E. (2010). EMINIM: an adaptive and memory-efficient algorithm for genotype imputation. J. Comput. Biol. *17*, 547–560.

49. Yalcin, B., Flint, J., and Mott, R. (2005). Using progenitor strain information to identify quantitative trait nucleotides in outbred mice. Genetics *171*, 673–681.

50. Keane, T.M., Goodstadt, L., Danecek, P., White, M.A., Wong, K., Yalcin, B., Heger, A., Agam, A., Slater, G., Goodson, M., et al. (2011). Mouse genomic variation and its effect on phenotypes and gene regulation. Nature *477*, 289–294.

51. Zhou, X., and Stephens, M. (2012). Genome-wide efficient mixed-model analysis for association studies. Nat. Genet. *44*, 821–824.

52. Zhou, X., and Stephens, M. (2014). Efficient multivariate linear mixed model algorithms for genome-wide association studies. Nat. Methods *11*, 407–409.

53. Han, B., and Eskin, E. (2011). Random-effects model aimed at discovering associations in meta-analysis of genome-wide association studies. Am. J. Hum. Genet. *88*, 586–598.

54. Han, B., and Eskin, E. (2012). Interpreting meta-analyses of genome-wide association studies. PLoS Genet. *8*, e1002555.

55. Yang, J., Lee, S.H., Goddard, M.E., and Visscher, P.M. (2011). GCTA: a tool for genome-wide complex trait analysis. Am. J. Hum. Genet. *88*, 76–82.

56. Bennett, B.J., Farber, C.R., Orozco, L., Kang, H.M., Ghazalpour, A., Siemers, N., Neubauer, M., Neuhaus, I., Yordanova, R., Guan, B., et al. (2010). A high-resolution association mapping panel for the dissection of complex traits in mice. Genome Res. *20*, 281–290.

57. Zou, J., Gopalakrishnan, S., Parker, C.C., Nicod, J., Mott, R., Cai, N., Lionikas, A., Davies, R.W., Palmer, A.A., and Flint, J. (2022). Analysis of Independent Cohorts of Outbred CFW Mice Reveals Novel Loci for Behavioral and Physiological Traits and Identifies Factors Determining Reproducibility. G3 (Bethesda) *12*, jkab394.

58. Nolan, M.F., Malleret, G., Dudman, J.T., Buhl, D.L., Santoro, B., Gibbs, E., Vronskaya, S., Buzsáki, G., Siegelbaum, S.A., Kandel, E.R., and Morozov, A. (2004). A behavioral role for dendritic integration: HCN1 channels constrain spatial memory and plasticity at inputs to distal dendrites of CA1 pyramidal neurons. Cell *119*, 719–732.

59. Pruim, R.J., Welch, R.P., Sanna, S., Teslovich, T.M., Chines, P.S., Gliedt, T.P., Boehnke, M., Abecasis, G.R., and Willer, C.J. (2010). LocusZoom: regional visualization of genome-wide association scan results. Bioinformatics *26*, 2336–2337.

60. Ng, L., Bernard, A., Lau, C., Overly, C.C., Dong, H.W., Kuan, C., Pathak, S., Sunkin, S.M., Dang, C., Bohland, J.W., et al. (2009). An anatomic gene expression atlas of the adult mouse brain. Nat. Neurosci. *12*, 356–362.

61. Yue, F., Cheng, Y., Breschi, A., Vierstra, J., Wu, W., Ryba, T., Sandstrom, R., Ma, Z., Davis, C., Pope, B.D., et al. (2014). A comparative encyclopedia of DNA elements in the mouse genome. Nature *515*, 355–364.

62. Ahrens, S., Wu, M.V., Furlan, A., Hwang, G.R., Paik, R., Li, H., Penzo, M.A., Tollkuhn, J., and Li, B. (2018). A Central Extended Amygdala Circuit That Modulates Anxiety. J. Neurosci. *38*, 5567–5583.

63. Levitan, D., Liu, C., Yang, T., Shima, Y., Lin, J.Y., Wachutka, J., Marrero, Y., Ali Marandi Ghoddousi, R., Veiga Beltrame, E.D., Richter, T.A., et al. (2020). Deletion of Stk11 and Fos in mouse BLA projection neurons alters intrinsic excitability and impairs formation of long-term aversive memory. Elife *9*, e61036.

64. McCullough, K.M., Daskalakis, N.P., Gafford, G., Morrison, F.G., and Ressler, K.J. (2018). Cell-type-specific interrogation of CeA Drd2 neurons to identify targets for pharmacological modulation of fear extinction. Transl. Psychiatry *8*, 164.

65. Lori, A., Maddox, S.A., Sharma, S., Andero, R., Ressler, K.J., and Smith, A.K. (2018). Dynamic Patterns of Threat-Associated Gene Expression in the Amygdala and Blood. Front. Psychiatry *9*, 778.

66. Chen, P.B., Kawaguchi, R., Blum, C., Achiro, J.M., Coppola, G., O'Dell, T.J., and Martin, K.C. (2017). Mapping Gene Expression in Excitatory Neurons during Hippocampal Late-Phase Long-Term Potentiation. Front. Mol. Neurosci. *10*, 39.

67. Yao, Z., van Velthoven, C.T.J., Nguyen, T.N., Goldy, J., Sedeno-Cortes, A.E., Baftizadeh, F., Bertagnolli, D., Casper, T., Chiang, M., Crichton, K., et al. (2021). A taxonomy of transcriptomic cell types across the isocortex and hippocampal formation. Cell *184*, 3222–3241.e26.

68. Catania, E.H., Pimenta, A., and Levitt, P. (2008). Genetic deletion of Lsamp causes exaggerated behavioral activation in novel environments. Behav. Brain Res. *188*, 380–390.

69. Qiu, S., Champagne, D.L., Peters, M., Catania, E.H., Weeber, E.J., Levitt, P., and Pimenta, A.F. (2010). Loss of limbic system-associated membrane protein leads to reduced hippocampal mineralocorticoid receptor expression, impaired synaptic plasticity, and spatial memory deficit. Biol. Psychiatry *68*, 197–204.

70. Luo, C., Rivkin, A., Zhou, J., Sandoval, J.P., Kurihara, L., Lucero, J., Castanon, R., Nery, J.R., Pinto-Duarte, A., Bui, B., et al. (2018). Robust single-cell DNA methylome profiling with snmC-seq2. Nat. Commun. *9*, 3824.

71. Preissl, S., Fang, R., Huang, H., Zhao, Y., Raviram, R., Gorkin, D.U., Zhang, Y., Sos, B.C., Afzal, V., Dickel, D.E., et al. (2018). Single-nucleus analysis of accessible chromatin in developing mouse forebrain reveals cell-type-specific transcriptional regulation. Nat. Neurosci. *21*, 432–439.

72. Liu, H., Zhou, J., Tian, W., Luo, C., Bartlett, A., Aldridge, A., Lucero, J., Osteen, J.K., Nery, J.R., Chen, H., et al. (2021). DNA methylation atlas of the mouse brain at single-cell resolution. Nature *598*, 120–128.

73. Love, M.I., Huber, W., and Anders, S. (2014). Moderated estimation of fold change and dispersion for RNA-seq data with DESeq2. Genome Biol. *15*, 550.

74. Guo, Y., Zhang, P., Sheng, Q., Zhao, S., and Hackett, T.A. (2016). lncRNA expression in the auditory forebrain during postnatal development. Gene *593*, 201–216.

75. Pimenta, A.F., Zhukareva, V., Barbe, M.F., Reinoso, B.S., Grimley, C., Henzel, W., Fischer, I., and Levitt, P. (1995). The limbic system-associated membrane protein is an Ig superfamily member that mediates selective neuronal growth and axon targeting. Neuron *15*, 287–297.

76. Tomita, H., Cornejo, F., Aranda-Pino, B., Woodard, C.L., Rioseco, C.C., Neel, B.G., Alvarez, A.R., Kaplan, D.R., Miller, F.D., and Cancino, G.I. (2020). The Protein Tyrosine Phosphatase Receptor Delta Regulates Developmental Neurogenesis. Cell Rep. *30*, 215–228.e5.

77. Pelkey, K.A., Barksdale, E., Craig, M.T., Yuan, X., Sukumaran, M., Vargish, G.A., Mitchell, R.M., Wyeth, M.S., Petralia, R.S., Chittajallu, R., et al. (2015). Pentraxins coordinate excitatory synapse maturation and circuit integration of parvalbumin interneurons. Neuron *85*, 1257–1272.

78. Irie, F., Okuno, M., Pasquale, E.B., and Yamaguchi, Y. (2005). EphrinB-EphB signalling regulates clathrin-mediated endocytosis through tyrosine phosphorylation of synaptojanin 1. Nat. Cell Biol. *7*, 501–509.

79. Schuske, K.R., Richmond, J.E., Matthies, D.S., Davis, W.S., Runz, S., Rube, D.A., van der Bliek, A.M., and Jorgensen, E.M. (2003). Endophilin is required for synaptic vesicle endocytosis by localizing synaptojanin. Neuron *40*, 749–762.

80. Bregin, A., Kaare, M., Jagomäe, T., Karis, K., Singh, K., Laugus, K., Innos, J., Leidmaa, E., Heinla, I., Visnapuu, T., et al. (2020). Expression and impact of Lsamp neural adhesion molecule in the serotonergic neurotransmission system. Pharmacol. Biochem. Behav. *198*, 173017.

81. Mann, F., Zhukareva, V., Pimenta, A., Levitt, P., and Bolz, J. (1998). Membrane-associated molecules guide limbic and nonlimbic thalamocortical projections. J. Neurosci. *18*, 9409–9419.

82. Chapman, G., Shanmugalingam, U., and Smith, P.D. (2019). The Role of Neuronal Pentraxin 2 (NP2) in Regulating Glutamatergic Signaling and Neuropathology. Front. Cell. Neurosci. *13*, 575.

83. Chang, S., Bok, P., Tsai, C.Y., Sun, C.P., Liu, H., Deussing, J.M., and Huang, G.J. (2018). NPTX2 is a key component in the regulation of anxiety. Neuropsychopharmacology *43*, 1943–1953.

84. Reutens, A.T., and Begley, C.G. (2002). Endophilin-1: a multifunctional protein. Int. J. Biochem. Cell Biol. *34*, 1173–1177.

85. Pechstein, A., Gerth, F., Milosevic, I., Jäpel, M., Eichhorn-Grünig, M., Vorontsova, O., Bacetic, J., Maritzen, T., Shupliakov, O., Freund, C., and Haucke, V. (2015). Vesicle uncoating regulated by SH3-SH3 domain-mediated complex formation between endophilin and intersectin at synapses. EMBO Rep. *16*, 232–239.

86. Gowrisankaran, S., Houy, S., Del Castillo, J.G.P., Steubler, V., Gelker, M., Kroll, J., Pinheiro, P.S., Schwitters, D., Halbsgut, N., Pechstein, A., et al. (2020). Endophilin-A coordinates priming and fusion of neurosecretory vesicles via intersectin. Nat. Commun. *11*, 1266.

87. Flint, J., Valdar, W., Shifman, S., and Mott, R. (2005). Strategies for mapping and cloning quantitative trait genes in rodents. Nat. Rev. Genet. *6*, 271–286.

88. Makino, K., and Ishikawa, A. (2018). Genetic identification of Ly75 as a novel quantitative trait gene for resistance to obesity in mice. Sci. Rep. *8*, 17658.

89. Stringer, C., Pachitariu, M., Steinmetz, N., Carandini, M., and Harris, K.D. (2019). High-dimensional geometry of population responses in visual cortex. Nature 571, 361–365.

90. DiCarlo, J.J., Zoccolan, D., and Rust, N.C. (2012). How does the brain solve visual object recognition? Neuron 73, 415–434.

91. Bugeon, S., Duffield, J., Dipoppa, M., Ritoux, A., Prankerd, I., Nicoloutso-poulos, D., Orme, D., Shinn, M., Peng, H., Forrest, H., et al. (2022). A transcriptomic axis predicts state modulation of cortical interneurons. Nature 607, 330–338.

92. Lovett-Barron, M., Andalman, A.S., Allen, W.E., Vesuna, S., Kauvar, I., Burns, V.M., and Deisseroth, K. (2017). Ancestral Circuits for the Coordinated Modulation of Brain State. Cell 171, 1411–1423.e17.

93. Schneider-Mizell, C.M., Bodor, A.L., Collman, F., Brittain, D., Bleckert, A., Dorkenwald, S., Turner, N.L., Macrina, T., Lee, K., Lu, R., et al. (2021). Structure and function of axo-axonic inhibition. Elife 10, e73783.

94. Flint, J., Heffel, M.G., Chen, Z., Mefford, J., Marcus, E., Chen, P.B., Ernst, J., and Luo, C. (2023). Single-cell methylation analysis of brain tissue prioritizes mutations that alter transcription. Cell Genom 3, 100454.

95. Krueger, F., and Andrews, S.R. (2011). Bismark: a flexible aligner and methylation caller for Bisulfite-Seq applications. Bioinformatics 27, 1571–1572.

96. Stuart, T., Butler, A., Hoffman, P., Hafemeister, C., Papalexi, E., Mauck, W.M., 3rd, Hao, Y., Stoeckius, M., Smibert, P., and Satija, R. (2019). Comprehensive Integration of Single-Cell Data. Cell 177, 1888–1902.e21.

97. Stuart, T., Srivastava, A., Madad, S., Lareau, C.A., and Satija, R. (2021). Single-cell chromatin state analysis with Signac. Nat. Methods 18, 1333–1341.

98. Zhang, Y., Liu, T., Meyer, C.A., Eeckhoute, J., Johnson, D.S., Bernstein, B.E., Nusbaum, C., Myers, R.M., Brown, M., Li, W., and Liu, X.S. (2008). Model-based analysis of ChIP-Seq (MACS). Genome Biol. 9, R137.

99. McGinnis, C.S., Murrow, L.M., and Gartner, Z.J. (2019). DoubletFinder: Doublet Detection in Single-Cell RNA Sequencing Data Using Artificial Nearest Neighbors. Cell Syst. 8, 329–337.e4.

100. Wolf, F.A., Angerer, P., and Theis, F.J. (2018). SCANPY: large-scale single-cell gene expression data analysis. Genome Biol 19, 15.

101. Korsunsky, I., Millard, N., Fan, J., Slowikowski, K., Zhang, F., Wei, K., Baglaenko, Y., Brenner, M., Loh, P.R., and Raychaudhuri, S. (2019). Fast, sensitive and accurate integration of single-cell data with Harmony. Nat Methods 16, 1289–1296.

102. Hafemeister, C., and Satija, R. (2019). Normalization and variance stabilization of single-cell RNA-seq data using regularized negative binomial regression. Genome Biol. 20, 296.

103. Purcell, S., Neale, B., Todd-Brown, K., Thomas, L., Ferreira, M.A.R., Bender, D., Maller, J., Sklar, P., de Bakker, P.I.W., Daly, M.J., and Sham, P.C. (2007). PLINK: a tool set for whole-genome association

and population-based linkage analyses. Am. J. Hum. Genet. 81, 559–575.

104. Valdar, W., Solberg, L.C., Gauguier, D., Cookson, W.O., Rawlins, J.N.P., Mott, R., and Flint, J. (2006). Genetic and environmental effects on complex traits in mice. Genetics 174, 959–984.

105. Srivastava, A., Morgan, A.P., Najarian, M.L., Sarsani, V.K., Sigmon, J.S., Shorter, J.R., Kashfeen, A., McMullan, R.C., Williams, L.H., Giusti-Rodríguez, P., et al. (2017). Genomes of the Mouse Collaborative Cross. Genetics 206, 537–556.

106. Shifman, S., Bell, J.T., Copley, R.R., Taylor, M.S., Williams, R.W., Mott, R., and Flint, J. (2006). A High-Resolution Single Nucleotide Polymorphism Genetic Map of the Mouse Genome. PLoS Biol. 4, e395.

107. Morgan, A.P., Fu, C.P., Kao, C.Y., Welsh, C.E., Didion, J.P., Yadgary, L., Hyacinth, L., Ferris, M.T., Bell, T.A., Miller, D.R., et al. (2015). The Mouse Universal Genotyping Array: From Substrains to Subspecies. G3 (Bethesda) 6, 263–279.

108. Kirby, A., Kang, H.M., Wade, C.M., Cotsapas, C., Kostem, E., Han, B., Furlotte, N., Kang, E.Y., Rivas, M., Bogue, M.A., et al. (2010). Fine mapping in 94 inbred mouse strains using a high-density haplotype resource. Genetics 185, 1081–1095.

109. Howie, B.N., Donnelly, P., and Marchini, J. (2009). A flexible and accurate genotype imputation method for the next generation of genome-wide association studies. PLoS Genet. 5, e1000529.

110. Ashbrook, D.G., Sasani, T., Maksimov, M., Gunturkun, M.H., Ma, N., Villani, F., Ren, Y., Rothschild, D., Chen, H., Lu, L., et al. (2022). Private and sub-family specific mutations of founder haplotypes in the BXD family reveal phenotypic consequences relevant to health and disease. Preprint at bioRxiv. https://doi.org/10.1101/2022.04.21.489063.

111. Doench, J.G., Hartenian, E., Graham, D.B., Tothova, Z., Hegde, M., Smith, I., Sullender, M., Ebert, B.L., Xavier, R.J., and Root, D.E. (2014). Rational design of highly active sgRNAs for CRISPR-Cas9-mediated gene inactivation. Nat. Biotechnol. 32, 1262–1267.

112. R Development Core Team (2010). R: A Language and Environment for Statistical Computing (R Foundation for Statistical Computing).

113. Yu, B., Zhang, Q., Lin, L., Zhou, X., Ma, W., Wen, S., Li, C., Wang, W., Wu, Q., Wang, X., and Li, X.M. (2023). Molecular and cellular evolution of the amygdala across species analyzed by single-nucleus transcriptome profiling. Cell Discov. 9, 19.

114. Jeong, H., Mendizabal, I., Berto, S., Chatterjee, P., Layman, T., Usui, N., Toriumi, K., Douglas, C., Singh, D., Huh, I., et al. (2021). Evolution of DNA methylation in the human brain. Nat. Commun. 12, 2021.

115. Liu, H., Zeng, Q., Zhou, J., Bartlett, A., Wang, B.A., Berube, P., Tian, W., Kenworthy, M., Altshul, J., Nery, J.R., et al. (2023). Single-cell DNA Methylome and 3D Multi-omic Atlas of the Adult Mouse Brain. Preprint at bioRxiv. https://doi.org/10.1038/s41586-023-06805-y.

116. Bürkner, P.C. (2017). brms: An R Package for Bayesian Multilevel Models Using Stan. J. Stat. Software 80, 1–28.

STAR★METHODS

KEY RESOURCES TABLE

REAGENT or RESOURCE	SOURCE	IDENTIFIER
Antibodies		
NeuN-488	Millipore Sigma	MAB377X; RRID:AB_2149209
NeuN-405	Novus Biologicals	NBP1-92693AF405
Critical commercial assays		
Next GEM scATAC-Seq v1.1	10X Genomics	PN-1000175
Chromium Next GEM Automated Single Cell 3′ Library and Gel Bead Kit v3.1	10X Genomics	PN-100014
Deposited data		
snmC-seq2 data of 8 mouse strains, amygdala	This study	GEO: GSE262259
snATAC-seq data of 2 mouse strains, amygdala	This study	GEO: GSE262259
snRNA-seq data of 2 mouse strains, amygdala	This study	GEO: GSE262259
snmC-seq2 data of 8 mouse strains, vhippocampus	Flint et al.[94]	GEO: GSE245367
snATAC-seq data of 2 mouse strains, vhippocampus	Flint et al.[94]	GEO: GSE245367
snRNA-seq data of 2 mouse strains, vhippocampus	Flint et al.[94]	GEO: GSE245367
CRISPR mouse KO generation	This study	https://doi.org/10.6084/m9.figshare.25521283
Subsampling of single-nucleus RNA and ATAC sequencing data and significant genes detected	This study	https://doi.org/10.6084/m9.figshare.25521304
Experimental models: Organisms/strains		
C57BL/6J	JAX	Strain ID: 000664
DBA/2J	JAX	Strain ID: 000671
CAST/EiJ	JAX	Strain ID: 000928
FVB/NJ	JAX	Strain ID: 001800
A/J	JAX	Strain ID: 000646
WSB/EiJ	JAX	Strain ID: 001145
PWK/PhJ	JAX	Strain ID: 003715
BALB/cJ	JAX	Strain ID: 000651
C57BL/6J-Megf9-KO	This study	N/A
C57BL/6J-Emb- KO	This study	N/A
C57BL/6J-Hcn1-KO	This study	N/A
C57BL/6J-Ptprd-KO	This study	N/A
C57BL/6J-Lsamp-KO	This study	N/A
C57BL/6J-Nptx2-KO	This study	N/A
C57BL/6J-Stim2-KO	This study	N/A
C57BL/6J-Mrps30-KO	This study	N/A
C57BL/6J-Parp8-KO	This study	N/A
C57BL/6J-Psip1-KO	This study	N/A
C57BL/6J-Sh3gl2-KO	This study	N/A
C57BL/6J-Snapc3-KO	This study	N/A
C57BL/6J-Ttc39b-KO	This study	N/A
C57BL/6J-4933413L06Rik-KO	This study	N/A
Software and algorithms		
Cell Ranger V6.0.2	10X Genomics	https://www.10xgenomics.com/support/software/cell-ranger/downloads
Cell Ranger ATAC V2.0.0	10X Genomics	https://support.10xgenomics.com/single-cell-atac/software/downloads/latest
Bismark V0.20.0	Krueger and Andrews[95]	https://github.com/FelixKrueger/Bismark

(Continued on next page)

Continued

REAGENT or RESOURCE	SOURCE	IDENTIFIER
DESeq2 V1.34.0	Love et al.[73]	https://bioconductor.org/packages/release/bioc/html/DESeq2.html
Seurat 4.0.5	Stuart et al.[96]	https://github.com/satijalab/seurat
Signac 1.5.0	Stuart et al.[97]	https://github.com/stuart-lab/signac
Model-based Analysis for ChIP-Seq (MACS) V3.0.0a7	Zhang et al.[98]	https://github.com/macs3-project/MACS
DoubletFinder V2.0.3	McGinnis et al.[99]	https://github.com/chris-mcginnis-ucsf/DoubletFinder
Scanpy V1.9.3	Wolf et al.[100]	https://pypi.org/project/scanpy/
Harmony V0.0.9	Korsunsky et al.[101]	https://github.com/immunogenomics/harmony
SCTransform V0.3.2	Hafemeister et al.[102]	https://github.com/satijalab/sctransform
EMINIM Beta 1.01	Kang et al.[48]	http://genetics.cs.ucla.edu/eminim/index.html
GEMMA V0.94	Zhou and Stephens[51]	https://github.com/genetics-statistics/GEMMA
PLINK V1.90b3.38	Purcell et al.[103]	https://zzz.bwh.harvard.edu/plink
METASOFT V2.0.1	Han and Eskin[53]	http://genetics.cs.ucla.edu/meta_jemdoc/
GCTA V1.93.1	Yang et al.[55]	https://yanglab.westlake.edu.cn/software/gcta
Wrappers for genetic mapping and quantitative complementation in inbred mouse strains	This study	https://doi.org/10.5281/zenodo.10892164

RESOURCE AVAILABILITY

Lead contact
Further information and requests for reagents and resources should be directed to and will be fulfilled by the lead contact, Jonathan Flint (JFlint@mednet.ucla.edu).

Materials availability
All mutant KO animals are deposited as frozen sperm at the Transgenic and Genome Editing Core Facility at Augusta University. Ordering information can be found at https://doi.org/10.6084/m9.figshare.25521283.

Data and code availability
- Raw and processed sequencing data generated for this study were deposited to NCBI GEO/SRA with accession number GSE245367 and GSE262259 and are publicly available at the time of publication.
- Mapping data (including imputed genotypes of all mouse inbred strains and F1s, together with results from the meta-analysis of the three phenotypes) https://figshare.com/s/7fcb1eebfd9c607afd12.
- Detailed CRISPR KO mouse generation for each gene, including exon targeted, sgRNA sequences, genotyping primers, and DNA gel images https://doi.org/10.6084/m9.figshare.25521283.
- Knockout interaction data, including phenotypes and genotypes for all quantitative complementation tests https://figshare.com/s/cc86ed5777cb95b99cec.
- Processed single nucleus epigenetic and gene expression data https://figshare.com/s/39e1c671ec0dc09d5b27.
- All original code has been deposited at https://doi.org/10.5281/zenodo.10892164.

EXPERIMENTAL MODEL AND STUDY PARTICIPANT DETAILS

Mouse strains
All experimental procedures using live animals were approved by UCLA's Animal Care and Use Committee (protocol number ARC-2018-026). Male mice from eight inbred strains A/J, C57BL/6J, BALB/cJ, FVB/J, DBA/2J, WSB/EiJ, PWK/PhJ, and CAST/EiJ were purchased from Jackson Laboratories at 8 weeks of age and transferred to UCLA where they were kept for at least 7 days before tissue extraction. Animals were housed with *ad libitum* food and water in a 12 h light-dark cycle. Mutant KO animals were generated on a C57BL/6J background.

METHOD DETAILS

Mouse phenotyping and mapping

Published data were obtained from three sources: the Jackson Laboratory website (https://phenome.jax.org), the Gene Network website (https://genenetwork.org) and PubMed. PubMed articles were identified using search terms including 'fear', 'anxiety', 'elevated plus maze', and 'fear conditioning'. This identified 29 potentially useful datasets.[16–45]

Harmonizing phenotyping data for meta-analysis

To harmonize the phenotypic data for the meta-analysis, we had to deal with the heterogeneity of the datasets collected. Each experiment used different protocols, different testing equipment and often reported different, though related, assays. Different studies used different names for what was supposedly the same phenotype. For example, for fear conditioning some studies reported the time freezing,[26] other reported its opposite, the amount of activity.[19] Some recorded 3 min of freezing, some 5 min, or more. EPM behavior was recorded in apparatus of different dimensions, under different lighting conditions, at different times of day, all of which are known to affect behavior.[104]

To deal with this, after downloading data and examining what was most collected, we decided to use the time freezing during a 5-min period after exposure to an altered context (contextual freezing), and the mean time spent freezing during exposure to a conditioned stimulus (most usually a tone). For the elevated plus maze we used the number of entries into the open arms. We created a data dictionary to convert the different phenotype names to a common set, and this is provided in Table S2.

Some studies also provided information about sex and age, and we tested, using a linear model, whether there was an effect on phenotypes of either. Since we found no significant effects (at a 5% threshold after correcting for multiple testing) and since some studies did not provide this information, we did not include covariates in downstream analyses.

We examined the relationship between phenotypes from different studies in two ways. First, for each strain for each study we obtained the trait mean and then calculated the correlation between the same strains in different studies. Not every study tested the same strains, so although there were 42 possible pairwise comparisons for FC-context, only 30 comparisons could be carried out. One study (Palmer5) was dropped because of insufficient overlap in the strains used with other studies. There was a considerable range in the correlations between studies (from −0.04 to 0.93), though only 13 comparisons were significant (at a $p < 0.05$, uncorrected for multiple testing), in part reflecting differences in the variation in the number of strains in each comparison (from 3 to 31). In some cases, a pair of studies were correlated, but not with other studies (for example for the FC-cue phenotype, study Bolivar2 is correlated with Bothe-2005 (r = 0.85) but neither study was highly correlated with others).

As a second measure of the relationship between studies, we ordered the means of each strain, and ranked them. We then applied the order for one study to another to examine the extent to which studies agreed on the order of strain means. We decided to use the pattern of correlations to select studies for the genetic analysis, requiring the presence of more than 5 strains in common, and a positive correlation greater than 0.2 (though we did not require this to be significant since). The studies we chose, together with the number of animals and the phenotype names, is given in Table S1.

Behavioral phenotyping

Mice from the Mouse Diversity Panel (HMDP) were used for the behavioral analyses. Mice (n = 700) were obtained through Jackson Laboratory at approximately 60 days old and housed for a 14-day acclimation period prior to testing. Mice were housed in groups (3–4 per cage) under a 12h/12h day/night cycle with *ad libitum* access to food and water. Testing was carried out between 10 a.m. and 4 p.m. Auditory background stimulus in the form of white noise (80db) was delivered through overhead speakers. All protocols conformed to NIH Care and Use Guidelines and were approved by UCLA's Animal Care and Use Committee (protocol number ARC-2018-026).

Behavioral tests

All tests were completed at the Behavioral Testing Core at UCLA. Animals were handled for 5 days prior to experiments. The order of experiments for genetic mapping was EPM -> FC cue/context. EPM -> 7 days-> FC training -> 24 h -> FC context -> 24 h -> FC tone.

Elevated plus maze

Animals were placed into an elevated plus maze apparatus (arms 5 cm × 30 cm) for 5 min with 15 lux at the center. We measured time spent in open/closed arms, and total entries into open/closed.

Fear-conditioning

Mice were placed in the conditioning chamber (context A) for 3 min before the onset of the discrete conditioned stimulus. The parameters were as follows:
  Tone: pure tone, 2700Hz, 80dB, rise/fall 50, duration 30s.
  Shock: 0.75 mAmps, duration 1s, inter-trial interval 180s.

Animals were exposed to three pairings of the CS and US. After the CS-US pairings, the mice were left in the conditioning chamber for another 60 s and then placed back in their home cages. FC boxes and software to control the boxes were purchased from MedAssociates.

Fear-conditioning context test: 24 h after conditioning, mice were returned to the same context (context A) with no shock or tone and freezing was measured for 8 min.

Fear-conditioning cued test: 24 h after the context test, mice were placed in a novel context (context B) where, they are exposed to the same procedure as the training but without any shocks (3 min exposure followed by 3 CS-US pairings, with parameters equal to fear acquisition). Freezing was measured during the initial 3 min exposure, during tone, and during the inter-trial interval.

Behavioral analysis

Behavior was recorded digitally from a camera mounted above each test chamber at 30 FPS. Following the completion of experiments, each recorded EPM video was analyzed using ANY-maze for positional tracking of the animal along the apparatus. For EPM mapping we measured open arm entries, time spent in open arms, and closed arm. VideoFreeze (MedAssociates) was used to measure animal freezing in QC testing from recorded videos. Freezing was determined as an absence of all visible movement except that required for respiration; in VideoFreeze, we set the motion threshold to 18 au with a minimum freeze duration of 1 s (30 frames). Contextual fear was assessed by total freezing time over the first 3 min of the test. Cued fear was assessed by total freezing time in response to the presentation of the first, second, and third CS during ITI. One exception was with freezing measurements during genetic mapping with BXD lines. Due to the variable coat color across lines, we used ANY-maze for animal tracking and freezing measurements as it performed better than VideoFreeze.

Genotyping

Our starting point for genotyping each mouse strain was variant calls from sequencing reads for those strains that have been sequenced,[46,105] and genotypes from high density arrays for those that have not[106] (https://www.informatics.jax.org/). We confirmed genotypes in the BxD recombinant inbred lines by randomly choosing 24 lines and subjecting to genotyping them on the GigaMUGA mouse array (140 thousand SNPs).[107] This genotyping was done commercially (Neogen GeneSeek Operations, 4131 *N* 48th St. Lincoln, NE 68504). All lines were of the expected genotype.

Imputation of genotypes

We used imputation to generate a near complete set of genotyped markers for all strains. The highest density set of genotyped markers is that derived from 16 strains for which we have complete sequence data[46] but this does not include any recombinant inbreds and lacks some of the strains used for mapping. Since the missing strains are descendants of a small number of founder haplotypes,[106] we can impute the genotypes in the non-sequenced strains. Using genotypes from arrays as a scaffold[56–93,104–108] we imputed missing genotypes using data from sequenced animals. Most imputation algorithms are designed for fully outbred populations, where a key problem is correctly phasing haplotypes (e.g.,[109]). Alternative methods are needed for efficient imputation in mouse strains and so we used the software tool EMINIM,[48] which requires a reference file, containing strains with known haplotypes, and a target file for imputation, containing strains genotyped at some SNPs. We ran this with the recommended parameter settings for inbred mice given according to the software documentation.

We prepared these two files by placing strains that were genotyped at all SNPs in the reference file, while strains with one or more missing SNPs were placed in the target file. For the BXD mice, SNPs between genotype markers from the same founder haplotype were pre-filled due to the negligible likelihood of multiple recombination events between consecutive genotyped SNPs. This resulted in 27 reference strains and 227 target strains. We then ran EMINIM imputation on each chromosome separately and obtained calls on 16,767,664 SNPs (triallelic SNPs, constituting 1% of the total, were discarded). Since EMINIM outputs high confidence values for one of the alleles, we translated a 90% or higher confidence for an allele into a hard call for that allele, with lower confidence calls being called as missing. We combined these imputation results with the genotyped data. The rate of missing calls was less than 0.8% for 18 of 19 autosomal chromosomes (chromosome 19 had a missing call rate of 1.03%).

We validated the imputation results by comparing imputed calls to genotypes from sequenced BXD strains obtained from.[110] The sequence-derived set contained 4,325,552 SNPs, of which 3,812,095 variant sites overlapped with our imputation. Across all chromosomes, each BXD strain was imputed with between 93% and 99% accuracy. Imputation accuracy for all strains combined varied between 89% and 99% per chromosome, with 96.29% overall. Due to the pre-filling procedure described previously, this accuracy reflects only the most challenging SNPs to impute: those between genotyped SNPs from different founder haplotypes. When including the genotyped and pre-filled SNPs, the accuracy for each chromosome was greater than 99.64%.

We performed a second assessment of imputation accuracy by removing the C57BL/6J and DBA/2J strains from our reference panel, randomly masking 50% of the bases of those strains, and using the remaining inbred strains in the reference panel to impute the masked bases. Once again, we used EMINIM with its default inbred imputation parameter settings and translated a 90% or higher confidence call for an allele into a hard genotype call. Calls with less than 90% confidence were translated to a missing call, leading to a missing genotype rate of 0.09%–0.59% per chromosome. The accuracy of imputation on the masked bases was 95.6%–99.7% per chromosome, and 97.9% overall.

Genetic mapping

All phenotypes were mapped in a two-stage approach. First, we used a mixed model, implemented in GEMMA[51,52] (obtained from https://github.com/genetics-statistics/GEMMA), to map each study separately. Input files for GEMMA were generated using PLINK,[103] obtained from https://zzz.bwh.harvard.edu/plink. We used the PLINK binary format of the required files, including all alleles with a frequency greater than 10%. A genetic relationship matrix was generated using the command:

gemma -bfile input.file -gk -o kinship.file.

Mapping was carried out using the command:

gemma -bfile pl input.file -k kinship.file -lmm -o output.file.

After mapping with GEMMA, the results files were combined with purpose written perl scripts into a format suitable for meta-analysis with METASOFT.[53,54] METASOFT (downloaded from http://genetics.cs.ucla.edu/meta_jemdoc/) was invoked with the following command:

java -jar Metasoft.jar -input input.file -mvalue -output output.file.

GEMMA assigns effects to the minor allele, as determined by the.bim files from PLINK which means there is considerable variation between studies as to which allele gets an effect (due to allele frequency variation). After running each study though GEMMA we swapped alleles to the most common arrangement, before proceeding to the meta-analysis.

METASOFT calculates a genomic-control inflation factor for the mean effect (lambda_Mean Effect) and a genomic-control inflation factor for heterogeneity (lambda_heterogeneity). These values were calculated for each run, and the software was run a second time, to include the effect of these variables. For example:

java -jar Metasoft.jar -input input.file -mvalue -output output.file -lambda_hetero 2.738124 -lambda_mean 2.430179.

Significance threshold for the genome-wide association studies

Simulations to estimate the appropriate significance threshold were carried out using GCTA,[55] obtained from https://yanglab.westlake.edu.cn/software/gcta. Phenotypes were simulated using real genotype data under a simple additive genetic model. A set SNPs was chosen as the causal variants that were seen to have effects in the mapping studies. We obtained estimated effect sizes for these SNPs from GEMMA output files and converted the beta estimate from the linear model to the values required by GCTA using

$Beta\_gcta = beta\_orig * sqrt(2 * p * (1 - p))$

(where p is the allele frequency from the GEMMA output file)

Input SNP files were those used for the mapping with GEMMA. 1000 simulations were carried out using the command:

gcta64 –bfile input.SNP.file –simu-qt –simu-causal-loci causal.snplist –simu-hsq 0.2 –simu-rep 3 –out.

After simulating data for each component study, files were processed through GEMMA and METASOFT exactly as for the real data.

To investigate the contribution of genotype structure to the inflation seen in quantile-quantile plots we simulated data in the same way, but with no causal SNPs.

Generating knockout animals for QC testing

We identified genes lying within QTLs, and determine whether they are expressed in brain tissue from *in situ* hybridization data (Allen Brain Atlas,[60] the mouse ENCODE transcription dataset[61]), and RNA-seq data obtained from the following publications: [62–67] For ISH data from the Allen dataset, we looked for presence of expression. For ENCODE transcriptome data we set a cutoff for an RPKM >5 in at least one brain region category, and for RNA-seq studies we ranked expression of each gene and averaged across studies; any gene in the top 25% of all genes (or >rank 6000) was considered expressed. For the Allen institute scRNA-seq dataset, we only included sequencing data from cell type clusters from CA1-CA3 of the hippocampus. Genes that passed expression thresholds for all three datasets were included for further consideration.

Where an existing knockout had been successfully created for the gene, usually on a C57BL/6N background, we adopted the same design, targeting the same part of the gene but in the C57BL/6J strain. To generate each KO, we used a CRISPR-Cas9 genome editing approach. For each gene, two single guide RNA (sgRNA) were generated by Synthego Corp. (Redwood City, California, USA) for targeting, except for 4933413L06Rik where we carried out a knock-in with a single-stranded DNA synthesized by IDT, Inc (Coralville, Iowa, USA). Guide RNAs (gRNAs) were designed to maximize both efficiency and specificity scores.[111] The sgRNA and/or ssDNA, and Cas9 protein (Alt-R SpCas9 Nuclease V3 from IDT) were co-injected into zygotes of C57BL/6J mice (Jackson Laboratory, Stock#009086). After microinjection, zygotes were transferred into the oviduct of pseudo-pregnant Swiss Outbred mice (Jackson Laboratory, Stock#034608) to generate founder mice. Founder mice were obtained and confirmed by PCR genotyping and Sanger sequencing. The correctly targeted founders were bred with C57BL/6J mice, and PCR genotyping and Sanger sequencing were again performed to confirm germline transmission. We used quantitative PCR to confirm that the deletion affected abundance of RNA transcript in hippocampal tissue from F1 animals. Full descriptions of each knockout design, and sgRNA sequences are given at dx.doi.org/10.6084/m9.figshare.25521283. Genotyping primers are listed in Table S4.

Quantitative polymerase chain reactions

To confirm the effect of the deletion on RNA production at each locus we ran quantitative polymerase chain reactions using a standard RT–qPCR assay (Taqpath COVID-19 Combo Kit). We analyzed RNA extracted from the hippocampus of heterozygous knockouts on C57BL6/J animals. Primer sequences can be found in Table S5.

Quantitative complementation testing

We generated offspring from four crosses.[4] C57BL/6J animals were mated to DBA/2J, and to heterozygote C57BL/6J animals where one allele was the knockout. DBA/2J animals were also mated to the heterozygote knockout mice. This generated four groups: wildtype C57BL/6J, F1 DBA/2J/C57BL/6J (wildtype), heterozygote C57BL/6J knockouts, and F1 DBA/2J/C57BL/6J (knockout). All four groups were assayed for the relevant phenotypes associated with the QTL, using the phenotyping protocols described above.

Evidence that the gene is the QTL gene was then detected as a statistical 'cross' (*mutant* or *wildtype*) by 'strain' (DBA/2J or C57BL/6J) interaction in a linear model, using the R statistical programming language.[112] Batch and sex were included as covariates, using the R command

summary (lm (phenotype $\sim$ sex + batch + cross $*$ strain, data = data))

Ventral hippocampus microdissections

Adult male animals (Jackson Laboratories) were euthanized at 10–16 weeks old in an isoflurane chamber and decapitated. The brain was removed and the ventral region of the hippocampus was microdissected, snap frozen in dry ice, and stored at $-80°C$ until processing. Tissue from $\sim$2 animals were combined into a single tube and considered a replicate, with 2 replicates per strain for snmC-seq2, snRNA-seq, and snATAC-seq experiments.

Amygdala microdissections

Adult male animals (Jackson Laboratories) were euthanized at 10–16 weeks old in an isoflurane chamber and decapitated. The brain was removed and coronal brain slices containing amygdala tissue were generated on a 1mm brain matrix (World Precision Instruments). Amygdala tissue was micro-dissected from these slices under a dissecting scope in cold PBS, snap frozen in dry ice, and stored at -80 until processing. Tissue from $\sim$2 to 3 animals were combined into a single tube and considered a replicate, with 2 replicates per strain for snmC-seq2, snRNA-seq, and snATAC-seq experiments.

Generating snmC-seq2 libraries

We carried out snmC-seq2 on microdissected tissue as previously described.[70] Briefly, frozen tissue was homogenized into single nuclei suspensions with Dounce homogenization, then immediately sorted on into a 384-well plate with a FACSAria sorter (BD Biosciences) at the UCLA Flow Cytometry Core. We selected for a 75-25 enrichment of neuronal vs. non-neuronal nuclei during FACS sorting using NeuN-488/DAPI counterstains (Millipore Sigma MAB377X). Bisulfite conversion and single-cell methylome libraries were generated following this step.

Generating snRNA-seq libraries

Single nuclei suspension and library generation were completed at the Cedars Sinai Applied Genomics, Computation and Translational Core and followed the 10X protocol for the Chromium Next GEM Automated Single Cell 3′ Library and Gel Bead Kit v3.1 (cat# PN-100014) as described except for the following modifications:

Suspensions from cell nuclei were generated using the recommended method from the 10X scMultiome protocol (CG000375 Rev C) to lyse cells and obtain nuclei. Following single nuclei suspension generation, nuclei were counterstained for 7-AAD and NeuN-405 antibody (Novus Biologicals, 1:200) and sorted on a MACSQuant Tyto (Miltenyi Biotech) prior to GEM generation. We selected for a 75-25 split of NeuN+/7-AAD+ nuclei for neurons and NeuN-/7-AAD+ for non-neuronal nuclei respectively.

We captured $\sim$10,000 nuclei per genotype per region per replicate on a single 10X GEM chip. All downstream library preparation was done according to the 10X Genomics protocol (CG000286) and sequenced on a Novaseq 6000 with a target of $\sim$40-50k reads per nucleus.

Generating snATAC-seq libraries

Single nuclei suspension and library generation were completed at the Cedars Sinai AGCT core and followed the 10X protocol for Next GEM scATAC-Seq v1.1 (PN-1000175) as described except for the following modifications:

Nuclei suspensions were generated using the recommended method from the 10X scMultiome protocol (CG000375 Rev C) to lyse cells and obtain nuclei.

Following single nuclei suspension generation, nuclei were counterstained for 7-AAD and sorted on a MACSQuant Tyto prior to GEM generation. NeuN was not used for neuronal enrichment due to dye incompatibility between our NeuN antibody and a nuclear counterstain. After the sort, we carried out permeabilization of nuclei as per the protocol. We aimed to capture 10,000 nuclei per well x 8 wells, for a total of 80,000 nuclei over 8 total samples ($\sim$10,000 nuclei per genotype per region per replicate). All downstream library

preparation was done according to the 10X Genomics protocol (CG000209) and sequenced on a Novaseq 6000 with a target of >35k reads per nucleus.

QUANTIFICATION AND STATISTICAL ANALYSIS

Single-nucleus RNA sequencing data quality control and pre-processing

All quality control and pre-processing were done under the Seurat package framework.[96] Per biological sample, we filtered out cells that (1) fall below the 5th percentile of the total UMI counts (nCount_RNA) or the 5th percentile total number of unique genes expressed (nFeature_RNA) or 700 unique genes expressed, whichever was more stringent; (2) are over the 95th percentile quantile in terms of either the total UMI counts or the total number of unique genes expressed; (3) have larger than 5% mitochondria fraction (percent.mt).

Global coverage normalization: counts per million (CPM) was applied to each cell followed by log transformation ("LogNormalize"). We then projected cells from each biological sample to low dimensional space using principal components analysis (PCA) on highly variable features selected by Seurat. Potential doublets were identified and subsequently removed from the downstream analysis by DoubletFinder,[99] ran in the top 15 principal components space with the expected doublet rate set to the recommended amount from 10X genomics based on high quality yield volume.

Single-nucleus ATAC sequencing data quality control and pre-processing

All quality control and pre-processing were done under the Seurat and Signac package framework.[97] Per sample, we first used Model-based Analysis for ChIP-Seq (MACS) to call sample specific *de-novo* peaks from its fragments file.[98] We then merged sample-specific sets of peaks to a unified peaks set while removing peaks with length larger than 10000bp or smaller than 20bp. A unified peaks by cells count matrix was constructed from the fragments file while removing cells with lower than 200 peaks detected and peaks only present in less than 10 cells. Cells were filtered based on the following criteria: (1) appropriate number of non-duplicate, usable read-pairs (passed_filters from Cell Ranger's output singlecell.csv). Specifically, we set it to larger than 3000, 4000, 2500, and 5000 for the 2 BL6 and 2 DBA samples collected in the hippocampus region. Similarly, we set it to be larger than 7500, 5000, 7500, and 7500 for their amygdala counterpart. (2) number of fragments overlapping peaks (peak_region_fragments from Cell Ranger's output singlecell.csv) falls within the 5th percentile and the 95th percentile. (3) ratio of fragments overlapping peaks over the total number of non-duplicate, usable read-pairs falls within the 5th percentile and the 95th percentile. (4) nucleosome_signal: the ratio of fragments between 147 bp and 294 bp (mononucleosome) to fragments <147 bp (nucleosome-free) is smaller than 4 (5) TSS enrichment score is larger than 2. We did not include a filter for ratio of peaks in black list regions over the total number of non-duplicate, usable read-pairs as this was removed during the construction of the DBA SNP-swapped reference genome. We normalized the count data with Text Frequency Inverse Document Frequency (RunTFIDF) and performed Singular Value decomposition (RunSVD) on top 90% informative features selected by Signac (FindTopFeatures). The first low dimensional embedding was excluded from downstream doublet detection and clustering analysis due to high correlation with sequencing depth. Potential doublets were identified and subsequently removed from downstream analysis by DoubletFinder,[99] ran on the 2nd - 11th low dimensional embedding with the expected doublet rate set to the recommended amount from 10X genomics based on high quality yield volume. Finally, we built a gene-by-cell transcriptional activity matrix that counts per cell, at the gene body and 2000bp upstream to capture the promoter region, the total number of ATAC-seq counts.

Single-nucleus methylation data quality control and pre-processing

Cells were filtered on the basis of several metadata metrics: (1) mCCC level <0.03; (2) global mCG level >0.5; (3) global mCH level <0.2; (4) total mapped reads >100,000; (5) Bismarck mapping rate >0.5; and 6 (percent genome covered >2). Methylation features were calculated as fractions of methylcytosine over total cytosine across gene bodies ± 2kb flanking regions and 100kb bins spanning the entire genome. Methylation features were further split into CG and CH methylation types. Features overlapping our methylation mm10 blacklist were removed. 100kb bin features were then filtered on minimum mean coverage >500 and maximum mean coverage <3000. Gene body features were filtered on minimum coverage >5 and all remaining features were normalized per cell using the beta binomial normalization technique in allcools.[72] Individual CpG sites were only counted when they had ≥5 reads covering the site.

Single-nucleus RNA sequencing data integration, clustering and annotation

Gene counts were normalized using SCTransform,[102] and regressed out percentage of reads from mitochondrial genes. We then integrated cells from all samples using reciprocal principal components analysis (rPCA) implemented in Seurat 4.0.5[96] on the top 5000 integration genes and in the top 30 reciprocal principal components space. For clustering, we standardized the integrated data, performed PCA on all integrated genes and ran *de-novo* Louvain clustering algorithm in the top 15 principal components space with resolution set to 0.1. Cluster markers that are conserved between the strains were called using non-parametric Wilcoxon rank-sum test and subsequently used for annotation. We annotated hippocampals clusters by manually checking conserved markers against the ALLEN BRAIN MAP's Mouse Whole Cortex and Hippocampus dataset. For cells collected in the amygdala, we performed a second round of analysis restricted to those identified to be neuronal in the initial annotation to increase our annotation resolution.

We used the same integration pipeline and parameters described above except when clustering we ran *de-novo* Louvain clustering algorithm in the top 25 principal components space with resolution set to 0.75, due to the increased expected complexity of cell types in this brain region. All clusters were first grouped into broad types of inhibitory or excitatory neurons except for one cluster that simultaneously expressed Gad2 and Slc17a7. We thus simply annotated it as "Neuronal" followed by its by cluster marker gene names. We also manually compared our clusters to those that were previously reported in amygdala,[113] and adapted their annotation for clusters with high concordance in top marker genes.

Single-nucleus ATAC sequencing data integration, clustering and annotation

We first jointly projected all cells' ATAC peak profile to uncorrected Latent Semantic Indexing (LSI) embeddings with TFIDF transformation followed by calculating SVD on the top 90% most informative peaks. Peak profile embeddings were then integrated in shared low dimensional space via integration anchors identified in the 2nd to 30th reciprocal LSI space as implemented in Signac 1.5.0. We then integrated cell transcriptional activity profiles by performing SCTransform after regressing out percentage of activity from mitochondrial genes and carried out rPCA integration on integration genes identified from the single-nucleus RNA experiment and in the top 10 reciprocal principal components. We transferred the single-nucleus RNA annotation onto the single-nucleus ATAC cells by linking the RNA's expression profile with ATAC's transcriptional activity profile through canonical correlation analysis (CCA) described in Seurat. Pairs of cells from each modality that are mutual nearest neighbors in the top 15 canonical components space were identified as "transfer anchors". "Anchors" were further filtered and weighted by distances in the integrated peak embeddings prior to imputing ATAC cells' annotation of cell type. For amygdala cells, after the initial assignment to cell type, we repeated the above-mentioned pipeline only on those cells predicted to be neuronal to obtain a set of higher resolution annotation. The second round of analysis was performed on integration genes identified from the subset of single-nucleus RNA data also categorized as neuronal.

Single-cell methylation data integration, clustering and annotation

We used the negative of the average mCH fraction of the gene body ± 2kb as the proxy of methylation cells' transcriptional activity as described previously.[72] We first integrated, across strains, single-nucleus methylation gene-body mCH profiles on RNA integration genes via "integration anchors" identified in the top 30 reciprocal PCA space. Gene body mCH profiles were then linked to single-nucleus RNA expression profiles via "transfer anchors" identified in the top 15 canonical components space. "Transfer anchors" were further filtered and weighted by distances in the integrated mCH embeddings prior to imputing methylation cells' annotation using their RNA counterpart as reference. For amygdala, we directly linked to the higher resolution annotation used on the neuronal cells in RNA. These served as our final annotation for all the neuronal cells in both hippocampus and amygdala. Since mCH methylation, used to construct the "transfer anchors", is largely not present in the non-neuronal population,[114] we further performed *de-novo* annotation on methylation cells using both the genome wide mCG and mCH fraction at 100kb as described previously.[115] Non-neuronal clusters were annotated by their canonical marker genes (gene-body hypo-methylation). These served as our final annotation for all the non-neuronal cells in both hippocampus and amygdala.

Co-embedding of single-nucleus RNA, single-nucleus ATAC, and single-nucleus methylation sequencing data

Both single-nucleus methylation and single-nucleus ATAC cells' expression profiles were imputed with previously computed "transfer anchors". All three modalities were merged on their integrated or imputed expression profiles, projected to low dimensional space via PCA, and visualized by UMAP (performed on the top 15 principal components).

Cell-type specific differential test for single-nucleus ATAC and single-nucleus RNA

We used DESeq2[73] for cell-type specific pseudobulk level differential expression analysis and differential accessibility analysis. Per cell type, raw counts were aggregated to replicate level and DESeq2 was run under default parameters to detect statistical evidence of strain differences. Any genes with no coverage in either or both strains were excluded.

Testing class and cell type effects on strain differences

We used the *brms* package in R to test for the effect of class analysis.[116] We defined a Bayesian model using *brms* with a negative binomial distribution for the number of significant differences (for RNA and ATAC data) or the number of mutations for methylation. We used up to eight chains and visually inspected the output to ensure chains were mixed. We used the following code to define the model:

$$\text{brm}(\text{significant\_difference} \sim 1 + (1 \mid \text{class} / \text{celltype}) + \log(\text{coverage}), \text{data} = \text{data}, \text{chain} = 8,$$

$$\text{control} = \text{list}(\text{adapt\_delta} = 0.95), \text{family} = \text{negbinomial}(\text{link} = ''\text{log}''))$$

Supplemental information

Complementation testing identifies genes

mediating effects at quantitative trait loci

underlying fear-related behavior

Patrick B. Chen, Rachel Chen, Nathan LaPierre, Zeyuan Chen, Joel Mefford, Emilie Marcus, Matthew G. Heffel, Daniela C. Soto, Jason Ernst, Chongyuan Luo, and Jonathan Flint

Supplemental Tables

Study ID	Name of measure in original data	EPM-open	FC-context	FC-cue	Source	Used	Sample size	Reference
Brown1	open_ent_EPM	1			JAX	YES	328	[1]
Flaherty1	EPM_open	1			JAX	YES	318	[2]
Milner-2008	EPM-open	1			Literature	YES	112	[3]
Schalkwyk1	entry_open_EPM	1			JAX	YES	86	[4]
Shin1	EPM_open	1			JAX	YES	123	[5]
UCLA-2023	EPM-open	1			UCLA	YES	333	This publication
Wahlsten1	EPM_open	1			JAX	YES	325	[6-7]
Brigman-2009	EPM-open	1			Gene Network		123	[8]
Brown1	open_ent_EZM	1			JAX		380	[1]
Carhuatanta-2014	EPM-open	1			Gene Network		307	[9]
Philip-2010	EPM-open	1			Gene Network		617	[10]
Yang-2008	EPM-open	1			Literature		142	[11]
Brigman-2009	FC-context		1		Gene Network	YES	111	[3]
Carhuatanta-2014	FC-context		1		Gene Network	YES	282	[9]
Owen-1997	FC-context		1		Literature	YES	300	[12]
UCLA-2023	FC-context		1		UCLA	YES	332	This publication
Yang-2008	FC-context		1		Literature	YES	150	[11]
Bolivar2	act_context_mean		1		JAX		289	[13]
Bothe-2005	FC-context		1		Literature		500	[14]
Knoll-2016	FC-context		1		Literature		721	[15]
Palmer1	freezing to context		1		JAX		462	[16]
Palmer3	freezing to context		1		JAX		319	[17]
Shin1	FC_memory		1		JAX		362	[5]
Smith-2011	ctx_imob		1		JAX		669	[18]
Brigman-2009	FC-cue			1	Gene Network	YES	116	[8]
Carhuatanta-2014	FC-cue			1	Gene Network	YES	301	[9]
Knoll-2016	FC-cue			1	Literature	YES	708	[4]
Owen-1997	FC-cue			1	Literature	YES	300	[12]
Smith-2011	cue_imob			1	JAX	YES	669	[18]
UCLA-2023	FC-cue			1	UCLA	YES	332	This publication
Yang-2008	FC-cue			1	Literature	YES	150	[11]
Bolivar2	act_cued_mean			1	JAX		289	[13]
Bothe-2005	FC-cue			1	Literature		500	[14]
Palmer1	freezing to tones			1	JAX		462	[16]
Palmer3	freezing to tones			1	JAX		319	[17]

Supplemental Table S2: Data identified from the published literature and websites for use in the meta-analysis for mapping fear related behavior, related to Figure 1. For the meta-analysis, this gives study ID, phenotype name used in the study, phenotype to which it was assigned in the meta-analysis (where EPM means elevated plus maze and FC means fear conditioning), source of the data, whether the data were included into the meta-analysis, and number of animals and a reference to the original publication.

trait	chr	start	end	max pos	size	logp	n. of genes	selected
EPM-open	1	8,051,126	12,843,641	12822766	4.79	5.38	23	NO
EPM-open	1	81,170,369	90,915,537	90906140	9.75	4.71	114	NO
EPM-open	1	107,003,663	107,107,513	107039384	0.10	5.44	2	NO
EPM-open	1	134,517,231	142,991,595	142876925	8.47	5.17	67	NO
EPM-open	1	157,544,700	159,401,857	158161029	1.86	7.82	10	NO
EPM-open	2	86,964,644	87,228,108	87226901	0.26	9.73	13	NO
EPM-open	2	99,960,104	104,091,211	100845037	4.13	5.28	30	NO
EPM-open	2	114,378,383	117,549,383	114639431	3.17	7.64	15	NO
EPM-open	2	130,308,391	132,695,042	132656944	2.39	6.73	54	NO
EPM-open	2	178,967,969	181,729,773	178969014	2.76	5.07	71	NO
EPM-open	3	10,977,446	11,422,508	11421316	0.45	5.61	0	NO
EPM-open	3	38,981,096	45,775,379	38995330	6.79	6.23	22	NO
EPM-open	3	57,159,935	62,350,184	62350182	5.19	8.30	40	NO
EPM-open	3	105,097,575	112,000,682	111438974	6.90	5.03	87	NO
EPM-open	3	123,188,658	123,396,053	123276372	0.21	6.12	3	NO
EPM-open	3	145,929,813	150,609,181	148545481	4.68	4.51	22	NO
EPM-open	4	33,005,779	40,497,077	33095253	7.49	4.64	41	NO
EPM-open	4	57,671,803	62,857,853	57671910	5.19	4.73	62	NO
EPM-open	4	76,119,560	85,680,047	76447340	9.56	6.13	24	NO
EPM-open	4	115,165,660	121,522,914	117736252	6.36	5.49	149	NO
EPM-open	4	137,887,832	145,481,723	138501861	7.59	6.37	143	NO
EPM-open	4	155,544,804	156,238,419	155968187	0.69	4.55	48	NO
EPM-open	5	54,144,189	54,263,530	54234453	0.12	13.15	0	YES
EPM-open	5	108,100,558	110,251,292	108100635	2.15	10.25	47	NO
EPM-open	5	126,174,260	126,355,761	126192582	0.18	8.67	0	NO
EPM-open	5	144,223,539	144,987,290	144233030	0.76	4.98	11	YES
EPM-open	6	22,443,939	25,909,081	23092121	3.47	11.37	21	NO
EPM-open	6	88,721,203	98,441,406	92702629	9.72	5.54	84	NO
EPM-open	6	115,361,899	116,527,763	116527093	1.17	11.10	25	NO
EPM-open	6	140,493,700	148,611,826	148609800	8.12	5.19	74	NO
EPM-open	7	26,633,267	32,815,915	32807189	6.18	6.78	199	NO
EPM-open	7	92,714,690	100,590,709	99781176	7.88	4.81	78	NO
EPM-open	8	47,424,796	49,191,404	49189891	1.77	5.45	12	NO
EPM-open	8	117,219,229	117,238,740	117238740	0.02	7.91	0	NO
EPM-open	9	37,046,757	42,684,188	41699149	5.64	5.50	143	NO
EPM-open	9	59,269,502	60,576,659	60415574	1.31	5.04	18	NO
EPM-open	10	3,982,409	7,993,140	7460347	4.01	6.37	31	NO
EPM-open	10	62,407,026	68,117,393	66257850	5.71	4.97	44	NO
EPM-open	10	87,467,449	87,595,552	87595101	0.13	5.12	2	NO
EPM-open	10	99,702,519	100,643,112	100180799	0.94	9.25	10	NO
EPM-open	10	115,061,969	116,129,037	116101513	1.07	6.47	11	NO

EPM-open	10	127,597,093	128,207,380	128207149	0.61	7.15	26	NO
EPM-open	11	31,617,205	33,045,751	31650378	1.43	6.48	23	NO
EPM-open	11	73,152,512	78,258,400	74973330	5.11	4.75	140	NO
EPM-open	11	92,514,551	102,328,161	96517839	9.81	4.95	329	NO
EPM-open	12	10,903,674	12,325,756	12280611	1.42	10.29	12	NO
EPM-open	12	24,801,558	24,941,020	24940968	0.14	6.21	2	NO
EPM-open	12	72,397,728	80,142,472	79653619	7.75	4.76	71	NO
EPM-open	12	91,547,374	98,556,066	91724133	7.01	4.60	12	NO
EPM-open	12	108,589,687	116,579,257	113828296	7.99	9.45	176	NO
EPM-open	13	64,041,193	64,320,793	64314535	0.28	7.15	7	NO
EPM-open	13	96,546,053	106,493,266	96581488	9.95	5.45	83	NO
EPM-open	14	76,541,966	77,890,188	76807687	1.35	5.42	9	NO
EPM-open	14	120,012,537	122,241,245	121836360	2.23	4.76	18	NO
EPM-open	15	4,581,923	5,987,339	5910696	1.41	11.75	10	NO
EPM-open	15	58,665,949	59,903,946	59903856	1.24	11.96	13	NO
EPM-open	15	71,640,419	71,928,936	71799081	0.29	5.59	2	NO
EPM-open	15	95,805,247	96,231,856	96231261	0.43	8.20	6	NO
EPM-open	16	6,116,010	8,344,551	8160532	2.23	5.49	1	NO
EPM-open	16	41,370,396	41,397,117	41370402	0.03	9.48	1	YES
EPM-open	16	51,739,855	57,287,996	53176660	5.55	12.38	26	NO
EPM-open	17	17,525,875	18,122,485	18119717	0.60	10.79	12	NO
EPM-open	17	35,025,170	42,556,420	37885007	7.53	7.52	197	NO
EPM-open	17	71,861,284	80,410,865	73349005	8.55	5.49	59	NO
EPM-open	17	90,988,935	91,039,920	91039814	0.05	6.63	1	NO
EPM-open	18	19,237,701	19,467,138	19303086	0.23	6.69	0	NO
EPM-open	18	34,269,862	34,328,458	34323952	0.06	4.71	1	NO
EPM-open	18	45,056,349	54,799,081	52676655	9.74	5.11	52	NO
EPM-open	18	65,182,153	65,755,343	65182284	0.57	5.85	8	NO
EPM-open	18	75,473,013	76,395,866	76223188	0.92	8.47	6	NO
EPM-open	19	10,791,445	16,546,950	14581483	5.76	5.26	127	NO
EPM-open	19	46,663,249	47,371,106	46664076	0.71	11.33	16	NO
FC-context	2	125,868,001	129,363,717	128363526	3.50	5.13	61	NO
FC-context	2	131,054,562	132,419,076	131419005	1.36	5.46	24	NO
FC-context	4	54,968,565	58,974,284	55968578	4.01	6.56	28	NO
FC-context	4	63,558,947	65,303,376	64099832	1.74	6.14	9	NO
FC-context	4	70,154,809	78,177,088	73444653	8.02	7.39	25	YES
FC-context	4	78,766,185	85,257,786	84257660	6.49	8.23	21	YES
FC-context	5	111,026,691	113,811,974	112810193	2.79	5.43	39	NO
FC-context	10	92,603,234	94,876,655	93603389	2.27	6.03	31	NO
FC-context	10	102,470,556	105,577,476	105191184	3.11	5.99	12	NO
FC-context	11	113,211,188	113,375,870	113360130	0.16	5.54	1	NO
FC-context	13	79,653,177	84,780,850	80662886	5.13	7.07	17	NO
FC-context	13	88,050,130	92,556,190	89050599	4.51	5.97	13	NO

FC-context	15	3,062,020	6,754,143	5753680	3.69	6.34	26	NO
FC-context	16	69,443,083	73,061,157	72061114	3.62	5.67	9	NO
FC-cue	2	157,505,101	159,522,386	158521915	2.02	5.96	26	NO
FC-cue	7	81,429,834	101,030,310	89412852	19.60	12.88	186	NO
FC-cue	7	125,083,067	127,084,850	126084800	2.00	5.07	57	NO
FC-cue	9	106,693,528	108,694,995	107693870	2.00	5.89	77	NO
FC-cue	10	13,700,072	15,703,556	14700119	2.00	5.16	8	NO
FC-cue	11	3,370,877	9,544,314	8532018	6.17	5.5	100	NO
FC-cue	13	78,196,122	82,295,567	81923446	4.10	8.22	10	NO
FC-cue	13	82,924,324	89,583,537	88583892	6.66	7.06	14	NO
FC-cue	13	92,130,558	95,554,450	93126201	3.42	7.46	35	NO
FC-cue	13	116,386,705	118,387,377	117819025	2.00	7.57	7	YES
FC-cue	14	40,646,127	43,530,172	41646248	2.88	5.39	37	NO
FC-cue	14	61,757,581	64,255,785	62757647	2.50	5.31	40	NO
FC-cue	14	71,846,334	72,909,269	72846442	1.06	6.21	4	NO
FC-cue	16	26,422,169	28,281,084	27304476	1.86	6.71	10	NO
FC-cue	19	32,762,251	35,307,221	34269128	2.54	5.44	30	NO

Supplemental Table S3: Quantitative trait loci for fear-related behavior, related to Figure 1. The table shows the traits mapped (EPM-open: entries into the open arms of the elevated plus maze, FC-context: freezing to the context in a fear conditioning experiment; FC-cue: freezing to the cue in a fear conditioning experiment); *chr*: chromosome; *start*: start of empirically defined 95% confidence interval of the locus; *end*: end of the 95% confidence interval; *max pos*: position of the marker that gave the maximum negative logarithm (base 10) of the association P-value at the locus; *size* : length of the QTL; *logp*: value of the maximum negative logarithm (base 10) of the association P-value; *n. of genes*: number of genes in the interval; *selected*: whether or not this interval was chosen for testing by quantitative complementation

Gene	Description	Sequence 5'-3'	Product (bp)
Megf9	Megf9-M-F	GGTCAGGCTCTGAGGGTAGA	Mu: 206
	Megf9-M-R	GGAATCCGTTCCAATGAACA	(WT: 817)
	Megf9-W-F	CACAGGGCAGTGTGATTGTC	WT: 474
Emb	Emb W-F	CTCCCTCTGCTGGCTCTTTA	WT: 384
	Emb M-R	TCGAAACTGTCATCCAGTGC	Mu: 246
	Emb W-R	ATGGACATTTTTCCCACGTC	
Hcn1	Hcn1-M-F	ATTTGGATCAAAGGCAAACA	Mu: 240
	Hcn1-M-R	CAGTTGGCTCAAATGATTCAGA	(WT: 1167)
	Hcn1-W-F	AAAGCTGGTTTGTGGTGGAC	WT: 377
Ptprd	Ptprd-M-F	GGGTTGGGCACTGAGAAGTA	Mu: 229
	Ptprd-M-R	R TTTTGACATCCATTTCCAAGG	(WT: 673)
	Ptprd-W-R	R TCTCCAAAAGTCCCCAAATG	WT: 475
Lsamp	Lsamp-M-F	GCCCTCTCAGAAATGTCACG	Mu: 176
	Lsamp-M-R	TCACCAGCACATGGAGTTTC	WT: 539
Nptx2	Nptx2-M-F	GAAGCCCAGTTTCCTTTCCT	Mu: 190
	Nptx2-M-R-2	GGAGGCCATCACAGTAAGGT	(WT: 976)
	Nptx2-W-R	GCTGACCTGTGTGCTCACTT	WT: 403
Stim2	Stim2-M-F	ATGGGATCCCTTCTCTCTGG	Mu: 233
	Stim2-M-R	CAACTTCACCTTCCGGCTAC	(Wt: 1486)
	Stim2-W-R	TGAGATGCCTCGGTTACCTC	Wt: 490
Mrps30	Mrps30 WT-F	TTCCATTGGTGGCTTAGAAAA	
	Mrps30 Mut-R	GCCATCATGAACAAACATGG	Mu: 219
	Mrps30 WT-R	AGGAATGCGTTCTTCACCAC	WT: 442
Parp8	Parp8 WT-F	CACCGAATCTCCAAAAATGG	
	Parp8 Mut-R	TTTACAATTTTCCAGGCTCCA	Mu: 246
	Parp8 WT-R	CGTGGTGATCCAGCTAACAG	WT: 396
Psip1	Psip1 WT-F	GGGAAGATGGGAGACAGACA	
	Psip1 Mut-R	CCAGTCCAGGTATGGCATTT	Mu: 218
	Psip1 WT-R	TGTCACATCCCACTTAAATTTTG	WT: 422
Sh3gl2	Sh3gl2 WT-F	TGGAGGAGAAACCTGTCACTG	
	Sh3gl2 Mut-R	ATGTGGCACCAAAGCCTTAC	Mu: 250
	Sh3gl2 WT-R	CTTACCTGGATTGGGTTGGA	WT: 397
Snapc3	Snapc3 WT-F	GGGATGGCTCAGTGGTTAGA	Mu: 215
	Snapc3 Mut-R	GGAACAGGGTGGTAGACAGG	
Ttc39b	Ttc39b WT-F	GGTGAATGAAACGGAGCAGT	
	Ttc39b Mut-R	TTTGCTGGAGAGCATTCTTTT	Mu: 237
	Ttc 39b WT-R	GCCCTTTCTGTCCAGGAACT	WT: 392
4933413L06Rik	Rik-KI-F	GTCACAAGGGCACATGTTCCACT	Mu: 556
	Rik-KI-R	CCCCCACTGCTCACCAC	WT: 434

Supplemental Table S4: Genotyping primers for mouse knock outs, related to STAR Methods. The table gives the sequence of primers used to genotype the CRISPR-engineered mouse knockouts, providing the names of the target genes, forward and reverse primers, and the sizes of the amplification products (Mu: knockout ; WT: wildtype).

Target Gene	Description	Sequence 5'-3'	Tm	Product Size (bp)	Target Exons	Deleted Exon in knock out
Ptprd	Ptprd-23-24-25-F	GCACTTTATAAGAATGGATCGAG	57.15	198	23-24-25	#22
	Ptprd-23-24-25-R	AATGAAGCAGCCAGTTCTGC	60.55			
Megf9	Megf9-4-5-F	CGTGTTCCGCAGTGACTTCT	61.45	105	4-5	#2
	Megf9-4-5-R	TATTGCAGTTCTGGCCTGTG	59.86			
Lsamp	Lsamp-3-4-F	ATGAGGGCAGCAATGTAACC	59	168	3-4	#2
	Lsamp-3-4-R	GGCAGCCTTGCACTCATATT	60			
Stim2	Stim2-9-10-F	TCCTCCCTGGACGAAGTAGA	59	226	9-10	#6-#7
	Stim2-9-10-R	CAGCAATAGGGTAGGGTGGA	60			
Nptx2	Nptx2-2-3-F	CGGAGCTGGAAGATGAGAAG	60	229	2-3	#1
	Nptx2-2-3-R	AGGCAGATGGTAAAGGCGTA	59			
Hcn1	Hcn1-4-5-F	GCCACAGCTTTGATCCAGTC	60.81	159	4-5	#2
	Hcn1-4-5-R	ATCGAAGATCTTGCCTTGGT	58.74			
Psip1	Psip1-4-5-F	GCAAACCAAATAAACGGAAAGGT	58.63	196	4-5	#3
	Psip1-4-5-R	GTCACATCCTCATTGCTGGC	59.26			
Emb	Emb-6-7-F	GAATGAGCTGGTTGTGCTGA	59.99	211	6-7	#5
	Emb-6-7-R	GTACCGGGGGACATTGTTTT	60.84			
Parp8	Parp8-24-25 F	GACGAGCCAGCTTCCAGTAG	60.16	164	24-25	#20,21,22
	Parp8-24-25 R	TTCGGGACAACCCATATCTC	59.75			
Mrps30	Mrps 30-4-5 F	CCATTGTTCAGACGGCAGTA	59.72	200	3-4	#2
	Mrps 30-4-5 R	GCTCCAGTCCAAGCAAAAG	59.99			
Ttc39b	Ttc39b-3-4-F	TTGTACCATGCGAGACCAAA	60.11	124	3-4	#2
	Ttc39b-3-4-R	TTCAGTGCCTCTGCACACTC	60.19			
Sh3gl2	Sh3gl2-4-5-F	CAGAGGCCATGCTCAAGTTC	60.94	157	4-5	#3
	Sh3gl2-4-5-R	AGATTCTGAAGGGGGTCGAT	59.9			
Snapc3	Snapc3-4-5-F	CCTGAAAACCCAGCAGACAT	60.11	192	4-5	#3
	Snapc3-4-5-R	GAATTCTCCACCGATCTGGA	60.01			
4933413L06Rik	RIK(5)-4-F-1	CAGCCTGTTTCCCAGTCATC	60.6	192	4	#1
	RIK(5)-4-R-1	AATGCTCTTTGGTGGCATT	59.5			

Supplemental Table S5: qPCR primers used to determine expression of the CRISPR targeted genes, related to STAR Methods. The table gives the sequence of primers used in the quantitative PCR testing of the knock-out animals, providing the names of the target genes, forward and reverse primers, the melting temperature (Tm), the product size, the exons amplified and the exon that is deleted in the CRISPR engineered mouse line.

RNA	Hippocampus			Amygdala			
Cell type	total	significant	pct	Cell type	total	significant	pct
Exc-CA1-Camk2d	18015	587	3.258	Exc-Abi3bp	18785	473	2.518
Exc-CA1-Fras1	18152	1149	6.330	Exc-Ebf2	13090	111	0.848
Exc-CA1-Galntl6	19739	1993	10.097	Exc-Strip2	5714	7	0.123
Exc-CA3	19562	1511	7.724	Exc-Tafa1	19527	940	4.814
Exc-Cdh12	13249	155	1.170	Exc-Tfap2c	8494	19	0.224
Exc-DG	20271	2236	11.031	Exc-Vwa5b1	19592	767	3.915
Exc-ENT	18376	1123	6.111	Inh-Drd2	13046	35	0.268
Exc-Gpc6	15946	526	3.299	Inh-Htr3a	14074	126	0.895
Inh-CGE	16845	399	2.369	Inh-Lamp5	12786	74	0.579
Inh-Lamp5	14426	229	1.587	Inh-Lypd6b	12946	78	0.603
Inh-MGE	17820	365	2.048	Inh-Nxph2	19945	164	0.822
NN-Astro	18340	466	2.541	Inh-Sst	18321	340	1.856
NN-MGC	13338	164	1.230	Inh-Tshz1	17989	28	0.156
NN-ODC	15986	601	3.760	Inh-Zfhx3	18812	107	0.569
NN-OPC	15579	384	2.465	NN-Astro	19206	570	2.968
NN-VLMC	11062	63	0.570	NN-Endo_SMCPeri	5506	6	0.109
CR-CR	11082	45	0.406	NN-Endo_VLMC	4373	86	1.967
				NN-MGC	13709	188	1.371
				NN-ODC	14315	348	2.431
				NN-OPC	16216	364	2.245
				NN-VLMC	8814	18	0.204

ATAC	Hippocampus			Amygdala			
Cell type	total	significant	pct	Cell type	total	significant	pct
Exc-CA1-Camk2d	274444	1176	0.429	Exc-Abi3bp	244313	325	0.133
Exc-CA1-Fras1	268808	1242	0.462	Exc-Ebf2	197530	52	0.026
Exc-CA1-Galntl6	277994	3637	1.308	Exc-Strip2	143706	9	0.006
Exc-CA3	277897	3296	1.186	Exc-Tafa1	251656	2755	1.095
Exc-Cdh12	162588	32	0.020	Exc-Tfap2c	82406	8	0.010
Exc-DG	277754	4282	1.542	Exc-Vwa5b1	248416	918	0.370
Exc-ENT	261482	690	0.264	Inh-Drd2	141913	22	0.016
Exc-Gpc6	230447	888	0.385	Inh-Htr3a	121437	19	0.016
Inh-CGE	218934	95	0.043	Inh-Lamp5	111249	23	0.021
Inh-Lamp5	158758	40	0.025	Inh-Lypd6b	100583	8	0.008
Inh-MGE	254528	32	0.013	Inh-Nxph2	246554	424	0.172
NN-Astro	51716	3	0.006	Inh-Sst	206133	85	0.041
NN-MGC	55630	9	0.016	Inh-Tshz1	243662	393	0.161
NN-ODC	38625	2	0.005	Inh-Zfhx3	242906	474	0.195
NN-OPC	47529	3	0.006	NN-Astro	48911	3	0.006
				NN-MGC	46732	5	0.011
				NN-ODC	28016	2	0.007

Methylation	Hippocampus				Amygdala		
Cell type	total	mutation	pct	Cell type	total	mutation	pct
Exc-CA1-Camk2d	591460	1051	0.178	Exc-Abi3bp	822415	547	0.067
Exc-CA1-Fras1	1012284	1737	0.172	Exc-Ebf2	2418	0	0.000
Exc-CA1-Galntl6	6761056	26464	0.391	Exc-Strip2	2267	0	0.000
Exc-CA3	3255884	9203	0.283	Exc-Tafa1	1.2E+07	46504	0.380
Exc-Cdh12	7485	110	1.470	Exc-Tfap2c	280	3	1.071
Exc-DG	14759665	81752	0.554	Exc-Vwa5b1	5264608	12172	0.231
Exc-ENT	739955	1176	0.159	Inh-Drd2	3085	0	0.000
Exc-Gpc6	200918	484	0.241	Inh-Htr3a	8419	1	0.012
Inh-CGE	15833	40	0.253	Inh-Lamp5	4167	0	0.000
Inh-Lamp5	12629	20	0.158	Inh-Lypd6b	5250	1	0.019
Inh-MGE	754092	578	0.077	Inh-Nxph2	3860176	7128	0.185
NN-Astro	5141	30	0.584	Inh-Sst	267290	205	0.077
NN-EC	436	3	0.688	Inh-Tshz1	1021024	1466	0.144
NN-MGC	93803	366	0.390	Inh-Zfhx3	1189382	1879	0.158
NN-ODC	1620528	1073	0.066	NN-Astro	91417	104	0.114
NN-OPC	29065	166	0.571	NN-MGC	17552	17	0.097
NN-VLMC	954	8	0.839	NN-ODC	71576	96	0.134
				NN-OPC	16264	52	0.320
				NN-VLMC	1232	8	0.649

Supplemental Table S7: The number of RNA species and ATAC sites that differed significantly between C57BL/6J and DBA/2J, and the number of methylation sites containing mutations that removed the methylated site, related to Figure 6. Significant differences were determined by exceeding an adjusted *p* value below a 5% FDR cutoff value, the default from the output of DESeq2). Data for each cell type is shown below for the two brain regions (hippocampus and amygdala), with counts of the significant species, and percentages of the total.

Modality	Class	Hippocampus	Amygdala
RNA	Excitatory	6.47	2.72
	Inhibitory	2.02	0.74
ATAC	Excitatory	0.75	0.35
	Inhibitory	0.03	0.10
Methylation	Excitatory	0.45	0.32
	Inhibitory	0.08	0.17

Supplemental Table S8: The weighted means of significant strain differences, expressed as a percentage, for the excitatory and inhibitory classes of cell type in the hippocampus and amygdala, related to Figure 6. Results are means of the excitatory and inhibitory cell types from Supplemental Table S7, weighted by the number of observations, showing that there appear to be more excitatory than inhibitory variable species. All differences are highly significant by Fisher's exact test P-values $P < 2e-16$.

Modality	Tissue	Deviance	P-value
RNA	Hippocampus	1291.6	<2.2e-16
	Amygdala	1282.2	<2.2e-16
ATAC	Hippocampus	12895.3	<2.2e-16
	Amygdala	8771.2	<2.2e-16
Methyl	Hippocampus	28295.7	<2.2e-16
	Amygdala	517.86	<2.2e-16

Supplemental Table S9: Cell type contributes to the number of significant differences, related to Figure 6. The relative contribution of sequence coverage and cell type was assessed by comparing the fit of two models. In one model we used a single predictor, sequence coverage, for the number of significant species. In the second model we added cell type as a predictor. The improvement in fit was tested using ANOVA. Results are highly significant, as shown by the deviance and associated P-values in the table.

Modality	Tissue	Predictor	Estimate	z-value	P-value
RNA	Hippocampus	Sequence coverage	6.15E-05	30.80	<2e-16
		Class	-8.27E-01	-28.11	<2e-16
	Amygdala	Sequence coverage	6.72E-06	5.10	3.48E-07
		Class	-3.99E-01	-13.46	<2e-16
ATAC	Hippocampus	Sequence coverage	3.64E-04	30.91	<2e-16
		Class	-2.20E+00	-50.03	<2e-16
	Amygdala	Sequence coverage	1.65E-04	6.92	4.53E-12
		Class	-9.51E-01	-35.44	<2e-16
Methyl	Hippocampus	Sequence coverage	1.08E-01	102.61	<2e-16
		Class	-9.06E-01	-31.96	<2e-16
	Amygdala	Sequence coverage	8.39E-02	56.54	<2e-16
		Class	-6.29E-01	-61.35	<2e-16

Supplemental Table S10: Results from a generalized linear model (the glm function in R), testing whether sequence coverage and class ("Inhibitory" or "Excitatory") predict whether RNA or ATAC sites were significant, and whether methylation sites were mutant or not (in each case coding outcomes as 1 or 0), related to Figure 6. The effect of class is relative to "Excitatory" and the direction for each modality is the same (negative, meaning that prediction is positive for "Excitatory"), and highly significant. Similar results were obtained using negative binomial distribution. P-values were well calibrated, as shown by creating an empirical distribution by randomly selecting the same number of transcripts as in the observed data for each cell type from the total set of transcripts in all cell types, while ensuring that a gene was selected only once for each cell type. Analysing the empirical data in the same way as the real data, using the generalized linear model to test whether sequence coverage and class ("Inhibitory" or "Excitatory") predicted the strain differences, confirmed that the P-values we obtained for the real data were significantly different from the empirical null distribution ($P < 0.0001$ in all cases).

Modality	Tissue	Level	Predictor	Estimate	Est. Error	Lower 95% CI	Upper 95% CI
RNA	HIPPOCAMPUS	Group	Class	0.68	0.56	0.02	2.09
			Class:celltype	0.52	0.15	0.32	0.89
		Population	Coverage	0.50	0.01	0.49	0.51
RNA	AMYGDALA	Group	Class	0.85	0.79	0.02	2.85
			Class:celltype	1.10	0.25	0.73	1.68
		Population	Coverage	0.38	0.01	0.36	0.39
ATAC	HIPPOCAMPUS	Group	Class	2.54	1.31	0.73	5.81
			Class:celltype	1.26	0.41	0.69	2.27
		Population	Coverage	0.60	0.02	0.56	0.63
ATAC	AMYGDALA	Group	Class	1.33	1.45	0.04	5.19
			Class:celltype	0.42	0.32	0.02	1.23
		Population	Coverage	0.70	0.14	0.44	0.97
Methylation	HIPPOCAMPUS	Group	Class	1.37	1.37	0.04	4.87
			Class:celltype	0.95	0.47	0.36	2.13
		Population	Coverage	2.12	0.31	1.52	2.74
Methylation	AMYGDALA	Group	Class	0.86	0.79	0.04	3.07
			Class:celltype	0.49	0.33	0.13	1.39
		Population	Coverage	2.45	0.44	1.62	3.30

Supplemental table S11: Contribution of cell type to the number of significant differences between excitatory and inhibitory neurons, related to Figure 6. The table shows the results of testing whether the number of strain differences are significantly different between the two cell type classes (excitatory and inhibitory) while considering the coverage difference and accounting for the different numbers of cell types in each class. Results are from a Bayesian model using the *brms* package [19] with a negative binomial distribution for the number of significant differences (for RNA and ATAC data) or the number of mutations (for methylation data). The model includes predictors for sequence *Coverage* and *Class* of cell type (italicized words refer to the terms in the table). Results are given for the two tissues (hippocampus and amygdala) and three epigenetic modalities (RNA, methylation and ATAC), reporting standard deviations for group-level effects (class and cell type nested within class) and estimates for population-level effects (sequence coverage). The two-sided 95% credible intervals (lower and upper 95% confidence interval (CI) based on quantiles are given. Results are from eight chains, each of 2,000 iterations of which the first 1,000 are warmup to calibrate the NUTS sampler. To reduce divergent transitions, adapt_delta was set to 0.95. Chain convergence was 1, as estimated from the potential scale reduction factor on split chains (Rhat = 1). Results show that the estimate for class for each tissue and each modality has confidence intervals that do not overlap zero and therefore can be regarded as significant.

Strain	Cell type	Total	Mutant sites	Percentage
A/J	Excitatory	13,085,362	1,285,640	9.83
	Inhibitory	2,700,028	53,309	1.97
	Non-neuronal	1,435,768	23,415	1.63
C57BL/6J	Excitatory	12,639,259	758,120	6
	Inhibitory	944,284	14,485	1.53
	Non-neuronal	989,433	16,513	1.67
BALB/cJ	Excitatory	12,388,844	1,213,199	9.79
	Inhibitory	2,811,830	59,446	2.11
	Non-neuronal	1,807,105	29,817	1.65
DBA/2J	Excitatory	12,424,446	1,013,242	8.16
	Inhibitory	1,232,573	20,534	1.67
	Non-neuronal	2,267,190	37,280	1.64
FVB/J	Excitatory	12,494,856	682,230	5.46
	Inhibitory	349,790	8,262	2.36
	Non-neuronal	979,704	16,955	1.73
PWK/PhJ	Excitatory	13,766,132	985,463	7.16
	Inhibitory	983,129	15,771	1.6
	Non-neuronal	270,084	9,609	3.56
WSB/EiJ	Excitatory	12,046,029	1,257,213	10.44
	Inhibitory	2,654,718	58,372	2.2
	Non-neuronal	2,382,166	41,153	1.73

Supplemental Table S12: Proportion of variant methylation sites in multiple strain comparison, related to Figure 6. Results from seven strain comparisons are shown (column 1), each time with CAST/EiJ as the outgroup, for excitatory neurons, inhibitory neurons and non-neuronal cell types. The total number of methylated sites is given for each strain comparison ('Total') in each cell type. The column headed 'mutant sites' lists the number of sites fully methylated in one strain but ablated in the other due to the presence of a mutation. The column headed 'pct' gives the percentage of mutant sites.

REFERENCES

1.   O'Leary, T.P., Gunn, R.K., and Brown, R.E. (2013). What are we measuring when we test strain differences in anxiety in mice? Behav Genet *43*, 34-50.

2.   Cook, M.N., Williams, R.W., and Flaherty, L. (2001). Anxiety-related behaviors in the elevated zero-maze are affected by genetic factors and retinal degeneration. Behav Neurosci *115*, 468-476.

3.   Milner, L.C., and Crabbe, J.C. (2008). Three murine anxiety models: results from multiple inbred strain comparisons. Genes Brain Behav *7*, 496-505.

4.   Lad, H.V., Liu, L., Paya-Cano, J.L., Parsons, M.J., Kember, R., Fernandes, C., and Schalkwyk, L.C. (2010). Behavioural battery testing: evaluation and behavioural outcomes in 8 inbred mouse strains. Physiol Behav *99*, 301-316.

5.   Keum, S., Park, J., Kim, A., Park, J., Kim, K.K., Jeong, J., and Shin, H.S. (2016). Variability in empathic fear response among 11 inbred strains of mice. Genes Brain Behav *15*, 231-242.

6.   Wahlsten, D., Metten, P., and Crabbe, J.C. (2003). Survey of 21 inbred mouse strains in two laboratories reveals that BTBR T/+ tf/tf has severely reduced hippocampal commissure and absent corpus callosum. Brain Res *971*, 47-54.

7.   Wahlsten, D., Bachmanov, A., Finn, D.A., and Crabbe, J.C. (2006). Stability of inbred mouse strain differences in behavior and brain size between laboratories and across decades. Proc Natl Acad Sci U S A *103*, 16364-16369.

8.   Brigman, J.L., Mathur, P., Lu, L., Williams, R.W., and Holmes, A. (2009). Genetic relationship between anxiety-related and fear-related behaviors in BXD recombinant inbred mice. Behav Pharmacol *20*, 204-209.

9.   Carhuatanta, K.A., Shea, C.J., Herman, J.P., and Jankord, R. (2014). Unique genetic loci identified for emotional behavior in control and chronic stress conditions. Front Behav Neurosci *8*, 341.

10.   Philip, V.M., Duvvuru, S., Gomero, B., Ansah, T.A., Blaha, C.D., Cook, M.N., Hamre, K.M., Lariviere, W.R., Matthews, D.B., Mittleman, G., *et al.* (2010). High-throughput behavioral phenotyping in the expanded panel of BXD recombinant inbred strains. Genes Brain Behav *9*, 129-159.

11.   Yang, R.J., Mozhui, K., Karlsson, R.M., Cameron, H.A., Williams, R.W., and Holmes, A. (2008). Variation in mouse basolateral amygdala volume is associated with differences in stress reactivity and fear learning. Neuropsychopharmacology *33*, 2595-2604.

12.   Owen, E.H., Christensen, S.C., Paylor, R., and Wehner, J.M. (1997). Identification of quantitative trait loci involved in contextual and auditory-cued fear conditioning in BXD recombinant inbred strains. Behavioral Neuroscience *111*, 292-300.

13.   Bolivar, V.J., Pooler, O., and Flaherty, L. (2001). Inbred strain variation in contextual and cued fear conditioning behavior. Mamm Genome *12*, 651-656.

14.   Bothe, G.W.M., Bolivar, V., Vedder, M.J., and Geistfeld, J.G. (2005). Behavioral differences among fourteen inbred mouse strains commonly used as disease models. Comparative Medicine *55*, 326-334.

15.   Knoll, A.T., Halladay, L.R., Holmes, A.J., and Levitt, P. (2016). Quantitative Trait Loci and a Novel Genetic Candidate for Fear Learning. J Neurosci *36*, 6258-6268.

16.   Ponder, C.A., Munoz, M., Gilliam, T.C., and Palmer, A.A. (2007). Genetic architecture of fear conditioning in chromosome substitution strains: relationship to measures of innate (unlearned) anxiety-like behavior. Mamm Genome *18*, 221-228.

17.   Sittig, L.J., Carbonetto, P., Engel, K.A., Krauss, K.S., Barrios-Camacho, C.M., and Palmer, A.A. (2016). Genetic Background Limits Generalizability of Genotype-Phenotype Relationships. Neuron *91*, 1253-1259.

18.   Park, C.C., Gale, G.D., de Jong, S., Ghazalpour, A., Bennett, B.J., Farber, C.R., Langfelder, P., Lin, A., Khan, A.H., Eskin, E*., et al.* (2011). Gene networks associated with conditional fear in mice identified using a systems genetics approach. BMC Syst Biol *5*, 43.

19.   Bürkner, P.C. (2017). brms: An R Package for Bayesian Multilevel Models Using Stan. Journal of Statistical Software *80*, 1-28.